An Examination of Site Response in Columbia, South Carolina: Sensitivity of Site Response to "Rock" Input Motion and the Utility of $V_s(30)$

Alanna Paige Lester

Thesis submitted to the faculty of the Virginia Polytechnic Institute and State University in partial fulfillment of the requirements for the degree of

Master of Science
in
Geosciences

Dr. Martin C. Chapman (chair)
Dr. James R. Martin
Dr. Gordon Matheson
Dr. J. Arthur Snoke

June 1, 2005
Blacksburg, VA

Keywords: Site Response, Strong Motion, Earthquake Hazard Analysis, Columbia, South Carolina, IBC 2000

An Examination of Site Response in Columbia, South Carolina: Sensitivity of Site Response to "Rock" Input Motion and the Utility of $V_s(30)$

Alanna Paige Lester

ABSTRACT:

This study examines the sensitivity of calculated site response in connection with alternative assumptions regarding input motions and procedures prescribed in the IBC 2000 building code, particularly the use of average shear wave velocity in the upper 30 meters as an index for engineering design response spectra. Site specific subsurface models are developed for four sites in and near Columbia, South Carolina using shear wave velocity measurements from cone penetrometer tests. The four sites are underlain by thin coastal plain sedimentary deposits, overlying high velocity Paleozoic crystalline rock. An equivalent-linear algorithm is used to estimate site response for vertically incident shear waves in a horizontally layered Earth model. Non-linear mechanical behavior of the soils is analyzed using previously published strain-dependent shear modulus and damping degradation models.

Two models for material beneath the investigated near-surface deposits are used: B-C outcrop conditions and hard rock outcrop conditions. The rock outcrop model is considered a geologically realistic model where a velocity gradient, representing a transition zone of partially weathered rock and fractured rock, overlies a rock half-space. Synthetic earthquake input motions are generated using the deaggregations from the 2002 National Seismic Hazard Maps, representing the characteristic Charleston source. The U. S. Geological Survey (2002) uniform hazard spectra are used to develop 2% in 50 year probability of exceedance input ground motions for both B-C boundary and hard rock outcrop conditions. An initial analysis was made for all sites using an 8 meter thick velocity gradient for the rock input model. Sensitivity of the models to uncertainty of the weathered zone thickness was assessed by randomizing the thickness of the velocity gradient. The effect of the velocity gradient representing the weathered rock zone increases site response at high frequencies.

Both models (B-C outcrop conditions and rock outcrop conditions) are compared with the International Building Code (IBC 2000) maximum credible earthquake spectra. The results for both models exceed the IBC 2000 spectra at some frequencies, between 3 and 10 Hz at all four sites. However, site 2, which classifies as a C site and is therefore assumed to be the most competent of the four sites according to IBC 2000 design procedures, has the highest calculated spectral acceleration of the four sites analyzed. Site 2 has the highest response because a low velocity zone exists at the bottom of the geotechnical profile in immediate contact with the higher velocity rock material, producing a very large impedance contrast. An important shortcoming of the IBC 2000 building code results from the fact that it does not account for cases in which there is a strong rock-soil velocity contrast at depth less than 30 meters. It is suggested that other site-specific parameters, specifically, depth to bedrock and near-surface impedance ratio, should be included in the IBC design procedures.

Acknowledgements

I wish to express my thanks to my advisor, Dr. Martin Chapman, who is an incredible role model and has made me a better scientist. Dr. Chapman also suggested the topic of my thesis and has been relentless in assisting me with my research project. I would also like to thank Dr. Snoke for his tireless instruction and advisement that, quite often, was requested at the drop of a hat. Also, thank you to Dr. Martin has been a great source of advisement for my research and encouragement. My thanks also go to Dr. Matheson, who was my unofficial mentor while I worked at Schnabel Engineering and has continued to advise me even after I left.

Thank you to the Geosciences Department at Virginia Tech who has funded me and provided guidance when I needed it. A big thank you to Connie Lowe, Ellen Mathena, and Richard Godbee, who are always willing to help.

I also want to acknowledge my immediate and extended family who gives me support whenever I need it and keep life interesting. A special thank you to my parents, Leo and Ginny, who truly are wonderful people. My gratitude also to my fellow graduate students and my friends who make life bearable. Thank you especially to Lee Perren who has been a source of encouragement and a wonderful friend.

Thank you finally to South Carolina Department of Transportation for partially funding my project.

Table of Contents

List of Illustrations

Introduction

It is well known that near-surface conditions can have a strong impact on the nature of ground motion from earthquakes. H.F. Reid (1910) comments on the effect of near-surface conditions on shaking intensity during the 1906 San Francisco earthquake:

> "Experience shows that the damage done by destructive earthquakes is much greater on alluvial soil than on solid rock. A glance at the isoseismal map No. 23 will show how well this was exemplified by the California earthquake. Probably the best example we have is the city of San Francisco itself, which is built variously on solid rock, on sand, on natural alluvium, and on 'made ground'. The description of the destruction done in the city…shows that within its limits the character of the foundation was a far more potent factor in determining the damage done than nearness to the fault-line."

The factors influencing earthquake ground motion at the surface of the Earth are generally divided into source, path, and site effects (Kramer, 1996, p. 345). Generally, source effects involve those processes that depend upon the orientation of faulting, the temporal nature of the slip along a fault, and material properties in the vicinity of the source. The path effect constitutes wave propagation effects that occur in crystalline material at depth in the Earth. Site effects are generally recognized to occur in the shallow subsurface when incident seismic waves encounter reduced seismic velocities near the surface. The effect involves a response to ground motion propagation that may alter the amplitude, frequency, and duration of incident strong ground motion at depth. The local site effect depends upon the arrangement and material properties of the subsurface sediments, surface topography and strength of the incoming seismic motion.

Earthquake resistant design procedures in the form of Building Codes have been used for many years. Most strong-motion data and building performance evaluations that are used as input for national building codes are from the seismically active regions of western North America; however, the seismic hazard estimates for some parts of the

central and eastern United States (CEUS) approach that of coastal California. In particular, major earthquakes have occurred in the Mississippi Valley and in South Carolina since 1800. These areas have very different geologic conditions than typically encountered in California. In both the Mississippi Embayment and in South Carolina, bedrock shear wave velocities are generally much greater than encountered in California. Site effects in the CEUS at high levels of strong motion intensity have not yet been instrumentally recorded.

This study will evaluate how the current building code in South Carolina, International Building Code 2000 (IBC 2000), would perform should another event like the Charleston 1886 magnitude 7 event occurred. Thin coastal plain sediments overlying the crystalline bedrock would affect the ground motion at Columbia.

In this study, a synthetic earthquake, that is a simulation of the Charleston 1886 M=7 event, is made based on the 2002 national probabilistic seismic hazard maps developed by Frankel et al. (1996, 2002). The subsurface conditions are defined from geotechnical data and a layered model is generated that describes the specific parameters of the sediments, such as velocity and density. Then, using the synthetic bedrock motion and layered subsurface model, a linear approximation to the non-linear response of the sites is estimated using the algorithm developed by Schnabel, Lysmer, and Seed (1972). The response spectra of the surface ground motions from Columbia, SC is compared to IBC 2000 design response spectra and illustrates the influence of subsurface materials, commonly called site response, on the incoming seismic waves.

Chapter 1: Geology and Seismic History of South Carolina

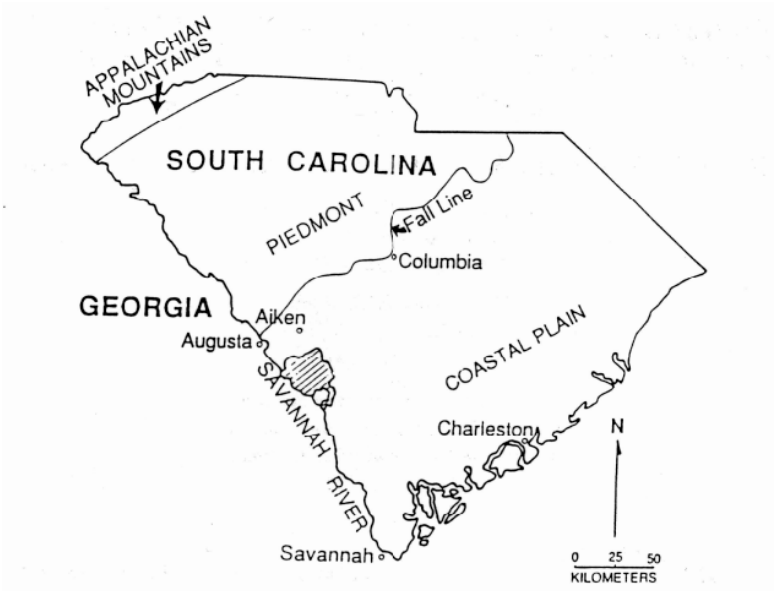

Figure 1.1: General physiographic map of South Carolina from Snipes et al., 1993, reproduced with permission of publisher.

As shown in figure 1.1, South Carolina contains three physiographic provinces: Blue Ridge, Piedmont, and Coastal Plain. A small portion of the Blue Ridge province lies in the northwest corner of the state. Geologists consider that the northeast trending Brevard fault zone is the boundary between the Blue Ridge and Piedmont provinces. The Blue Ridge province contains Precambrian and early Paleozoic age crystalline rock. The Piedmont consists of metamorphic and volcanic rocks that range in age from Paleozoic to middle Mesozoic. The northeast trending Fall Line is an erosional boundary that separates Piedmont crystalline and metamorphic rocks from Coastal Plain sediments as shown in figure 1.1. It lies near the center of the state and passes through Columbia, the state capitol. The Coastal Plain province has continental and marine deposits that are Holocene to Cretaceous in age and form a seaward thickening wedge. Thicknesses of the Coastal Plain sediments vary from zero at the Fall Line

and increases to more than 1 km in the southernmost part of the state. A generalized geologic map of the state is shown below in figure 1.2.

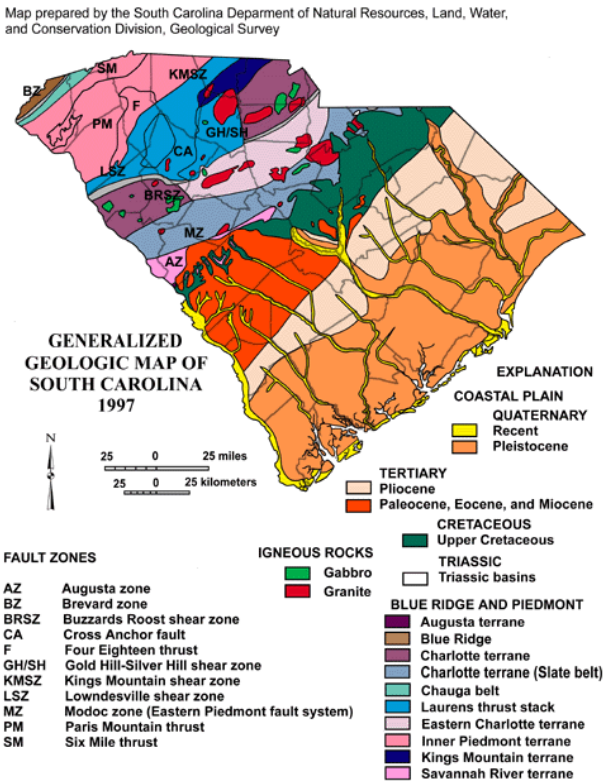

Figure 1.2: Generalized Geologic Map of South Carolina modified from Maybin and Nystrom, 1997, South Carolina Department of Natural Resources (used with permission).

A large scale seismic reflection study, conducted by the Consortium for Continental Reflection Profiling or COCORP, in 1979, found that the Blue Ridge and Piedmont provinces consist of allochthonous thrust sheets of crystalline Precambrian and Paleozoic rock (Cook et al., 1979). Also, a large package of late Paleozoic sedimentary rock underlies the crystalline thrust sheets.

A high resolution Vibroseis reflection profile acquired in preparation for the proposed Appalachian Ultra-Deep Core Hole (ADCOH) project in 1987, near the COCORP lines, found

that the Blue Ridge fault was not as deep as interpreted on the COCORP profile (Coruh et al., 1987). Other structures interpreted by Coruh et al.(1987) include a duplex of thrust faults within Paleozoic strata underlying the Blue Ridge fault and rifts in the Grenville Basement.

Several reflection seismic surveys in the Coastal Plain near the South Carolina coast consistently image a strong flat-lying or slightly dipping reflector that is commonly referred to as the "J" reflector and is interpreted as a Jurassic age basalt (Schilt et al., 1983; Hamilton et al., 1983; Behrendt et al., 1983). A Cretaceous age deposit, referred to as the "K" reflector, and the basement or "B" reflector, are also interpreted by Schilt et al. (1983) and Hamilton et al. (1983); however, these later reflectors are not present on all profiles throughout the coastal South Carolina area. Schilt et al. (1983), Hamilton et al. (1983), and Behrendt et al. (1983) discuss the details of recognized faults of various ages.

The Precambrian rocks of the Blue Ridge consist of amphibolite and granulate grade gneiss basement in large scale, low-angle stacked thrust sheets. Late Proterozoic graywacke, schist and amphibolite overlie the crystalline gneiss and originate from the metamorphism of deep water sedimentary deposits and dikes (Hatcher and Goldberg, 1991). A band of low grade metamorphic rocks bounds the Proterozoic rocks and is referred to as the Brevard fault zone (Reed et al.,1970, p. 261).

The Paleozoic age rocks of the Piedmont consist of four different northeast trending lithologic belts and are listed from the northwestern boundary of the Piedmont (marked by the Brevard fault zone) to the southeastern border of the Piedmont with the Coastal Plain (Fall Line): Inner Piedmont, Kings Mountain, Charlotte, and Carolina slate belts (Overstreet, 1970). The largest belt is the Inner Piedmont belt and contains greenschist to amphibolite grade rocks that include schist, amphibolite, gneiss, ultramafic and granite intrusions, metavolcanic, and

metasedimentary deposits (Horton and McConnell, 1991, p.44). The Kings Mountain lithologic belt includes schist, marble and quartzite. The Charlotte belt contains intrusive granitoid plutons and mafic dikes with metamorphosed sequences of sedimentary and volcanic deposits (Overstreet, 1970). The grade of metamorphism varies and is generally amphibolite grade. The Carolina Slate Belt is a low grade metamorphic belt consisting of amphibolite and schists.

Mesozoic rocks consisting of sedimentary deposits, basalt flows and dikes are found in a number of extensional fault-bounded basins within the Piedmont and beneath the Coastal Plain. Buried Mesozoic basins include the Florence basin (near Florence, SC), Dunbarton basin (near Aiken, SC), and Jedburg basin (near Jedburg, SC). Much of southern South Carolina, from Charleston to Savannah, and southcentral Georgia is underlain by extensive Mesozoic materials. This large area is referred to as the South Georgia basin. The Mesozoic sedimentary packages include siltstones, mudstones, sands and red beds (Olsen et al., 1991, p.142). The basalt flows can be very thick; however, they generally are not laterally extensive. Near Charleston, a deep corehole (Clubhouse Crossroads Corehole 1) recovered amygdaloidal basalt of Jurassic age from a depth of 750 to 792 meters (Rankin, 1977). Other cores exceeded 792 meters depth and found intermittent layers of basalt and a continuous layer of sedimentary redbeds underlying the basalt. Figure 1.3 shows a general geologic map of the South Carolina Coastal Plain deposits with the labeled location of Clubhouse Crossroads Corehole (Hazel et al., 1977).

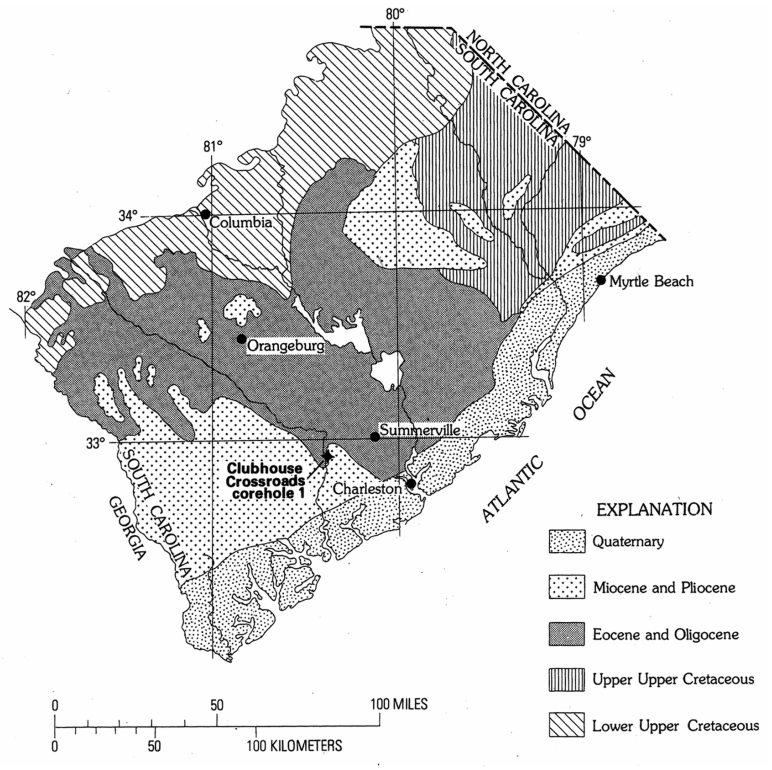

Figure 1.3: General Geologic map of Coastal Plain deposits from Hazel et al. (1977).

South Carolina lies within the North American Plate on the Atlantic Coast and in a passive margin tectonic setting. However, the coastal margin was quite active in the past. The first of four orogenic events was the Grenville orogeny that took place 1.1 Billion years ago in the Proterozoic, followed by rifting to form the Laurentian continent and Iaeptus Ocean. In the early to middle Ordovician and Silurian, subduction of an island arc occurred on the eastern margin of Laurentia (Taconic orogeny). This event accreted materials onto the eastern margin of Laurentia, which would later include the eastern United States (Hatcher and Goldberg, 1991, p. 13). Further accretion of island arc materials occurred during the Devonian (Acadian orogeny). Continental collision of Laurentia and Gondwanaland occurred in the Carboniferous to Permian and created the supercontinent, Pangea (Hatcher,1987). Rifting and break-up of Pangea began in the Triassic to form North America and the Atlantic Ocean. Faulting and extensive

sedimentation occurred in rift basins along the eastern margin of North America along with volcanism and igneous intrusion in the form of diabase dikes and basalt flows (Olsen et al., 1991, p. 170).

The southeastern margin of North America has been a passive continental margin since Cretaceous times. The Atlantic Coastal Plain has developed by erosion and deposition of the ancestral Appalachian mountains, beginning in the Cretaceous and continuing throughout the Cenozoic. Subtle post-Mesozoic deformation has occurred on the passive margin. As shown in figure 1.4, the modern coastline of South Carolina is bordered to the north by the Cape Fear arch whose fold axis is approximately parallel to the North Carolina state boundary. The margin has also been the site of earthquakes in Coastal South Carolina.

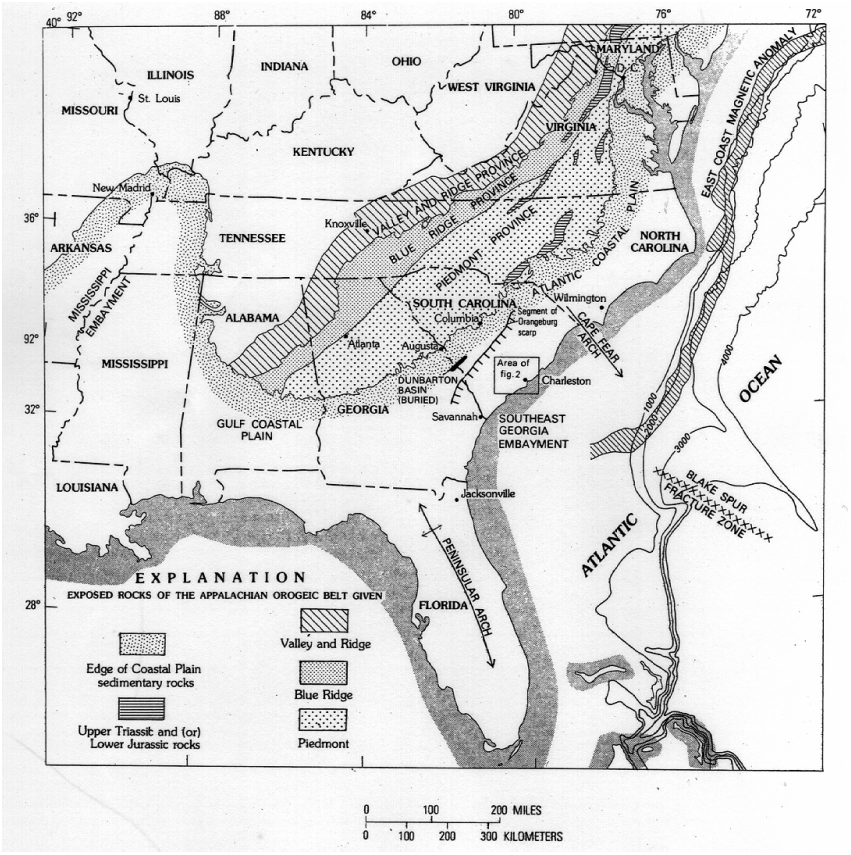

Figure 1.4: Southeastern United States map showing locations of various physiographic provinces and features from Rankin 1977.

Seismic History of South Carolina

Figure 1.5 shows the epicentral locations of earthquakes with magnitudes 3 to 7 occurring in South Carolina from 1689 to 2002, from the historical earthquake catalog and from instrumental data recorded in recent years by regional seismic networks. Notice that earthquakes have occurred across the state with varying magnitudes. There is a large cluster of earthquakes in the vicinity of Charleston that includes the 1886 magnitude 7 earthquake and more recent instrumentally located earthquakes.

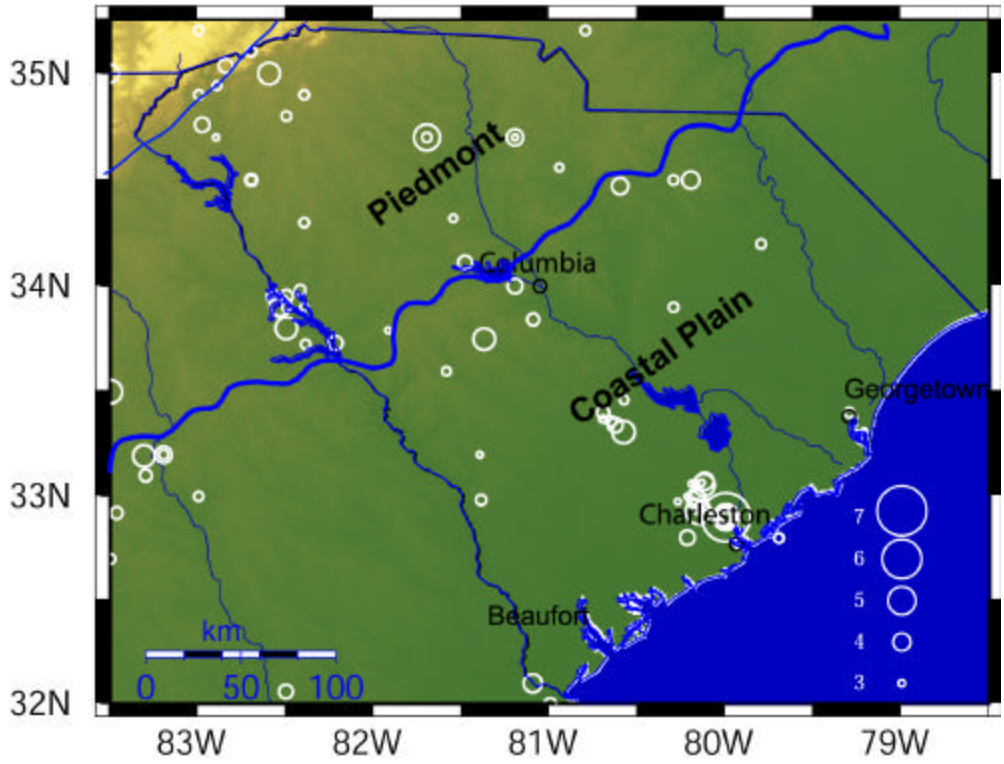

Figure 1.5: Historical epicenter locations of South Carolina from 1689 to 2002 (Southeastern U.S. Seismic Network Operators, 2004)

On August 31, 1886, Charleston and the surrounding area experienced a large magnitude earthquake. At the time of this earthquake, there were no instruments present in the area. Therefore, all of the magnitudes associated with this event are estimates based on felt area and intensity effects. The moment magnitude based on interpretation of historical intensity values include: 6.9 (Bakun and Hopper 2004), 7.0 (Bollinger 1977) and 7.3 (Johnston 1996).

Investigation and analysis of paleoliquefaction features in coastal South Carolina indicate that the average recurrence interval of a large magnitude event near Charleston is approximately every 500 to 600 years (Talwani and Schaffer, 2001). This paleoliquefaction evidence forms the basis for estimating return periods of large magnitude earthquakes in the Charleston area and has been incorporated in the latest version of the national seismic hazard maps (Frankel et al., 2002).

Dutton (1889) remarks upon the variable nature of shaking during the 1886 Charleston, SC earthquake. He draws special attention to the intensity of shaking in Columbia, SC and in other areas of South Carolina, North Carolina and Georgia that are situated in relatively thin sections of coastal plain sediments. He contrasts the strong shaking in those areas with lesser intensity motions at locations nearer the coast. In regard to North Carolina, Dutton (1889, p.329) states the following:

> "Throughout the State of North Carolina the vigor of the shocks was very great. Not a locality which has been interrogated has failed to report proofs of intensity sufficient to arouse and alarm the entire population. Not a village escaped minor damages, such as the loss of chimneys and plastering; and wherever brick structures exist the accounts of cracked walls are frequent. There is, however, a notable difference as a general rule between the eastern part of the State within the coastal region and the Piedmont and mountain region. It was notably less forcible in the coastal plain. In Wilmington, N.C., the shocks, though alarming everybody and shaking buildings with an energy that caused no little apprehension, did not produce the complete consternation which seized upon all classes in the towns and cities of the interior; and this statement holds good in full view of all qualification which might be expected to arise from the different distances of localities from the centrum."

Dutton goes on to state his belief that the great thickness of the coastal plain sediments along the coast resulted in less damage to structures than would have been the case were those structures sited on crystalline or metamorphic rocks that outcrop in the Piedmont. Chapman et al. (1990) demonstrate that Dutton's observations may be explained at least in part by anelastic absorption in the coastal plain deposits.

The fault location or mechanisms are not well defined for the large earthquakes that have occurred in coastal South Carolina. No surface fault rupture was found within the highest intensity area of the 1886 event (Dutton, 1889). Seismic reflection data from the 1886 epicentral area indicate a number of lithology changes with a gentle dip; however, the fault(s) responsible for the 1886 earthquake has not been conclusively identified (Yantis et al. 1983).

Several seismotectonic models have been proposed for the Charleston area. Talwani (1982) introduced the northeast trending Woodstock fault and the Ashley River fault that has a northwest orientation. Talwani (1999) revised his proposed faults and hypothesized that the Ashley River bisected the Woodstock fault to make a system of intersecting faults. The proposed faults in the Charleston area are also part of the proposed East Coast Fault System which has a north-northeast trend extending through Virginia, North Carolina, and South Carolina (Marple and Talwani 2000). Weems et al. (1997) proposed an additional fault in the Summerville area that trends east-northeast and connects to the Ashley River fault. The Charleston fault is another proposed fault that has a northwest trend and is not connected to the other proposed faults (Lennon 1986). Another fault is proposed by Weems and Lewis (2002) named the Adams Run fault which trends north and is hypothesized to be influenced by the Cape Fear arch and the Southeast Georgia embayment.

The geological evidence of paleoliquefaction features in coastal South Carolina (Talwani and Schaefer, 2001) points to repeated occurrence of moderate to major magnitude earthquakes in this area. This behavior is interpreted as indicative of "characteristic" earthquake activity (Youngs and Coppersmith, 1985; Schwartz and Coppersmith, 1984). In this model, repeating earthquakes of approximately the same magnitude occur within the same region.

Defining the magnitudes and tectonic environment of the paleoseismicity in coastal South Carolina is outside the scope of this study. However, treatment of this problem in the context of the National Seismic Hazard Maps is important because they define the basis for development of ground motions used in this study to investigate site response. In 2002, the National Seismic Hazard Maps were modified to include a complex logic tree for the characteristic Charleston source with variations in size of the fault area and magnitudes. The range of magnitudes, 6.8 to

7.5, is included in the source model with associated weighting and a smaller return interval of 550 years. The source for the Charleston characteristic source model is defined by a combination of two area source zones. The broad source zone encompasses the region of paleoliquefaction features in coastal South Carolina and the smaller area source represents the Woodstock fault scenario from Talwani (1982, 1999).

Chapter 2: Strong Motion Basics: One-Dimensional Site Response Analysis

Seismologists divide factors influencing earthquake ground motion into source, path, and site effects. The earthquake source describes the fault motion that depends on the fault geometry, rupture propagation along the fault, and slip velocity along the fault. The path effect involves transmission of the seismic waves to the near surface and will depend on density and velocity changes in the Earth. In this study, the path will represent the seismic wave propagation in crystalline or metamorphic rock with shear wave velocities approximately 3.5 kilometers per second or greater. The site effects are the influences of highly variable near-surface geology overlying the crystalline bedrock on the ground motion. Figure 2.1 shows a schematic of the parameters included in calculating surface motion in the frequency domain.

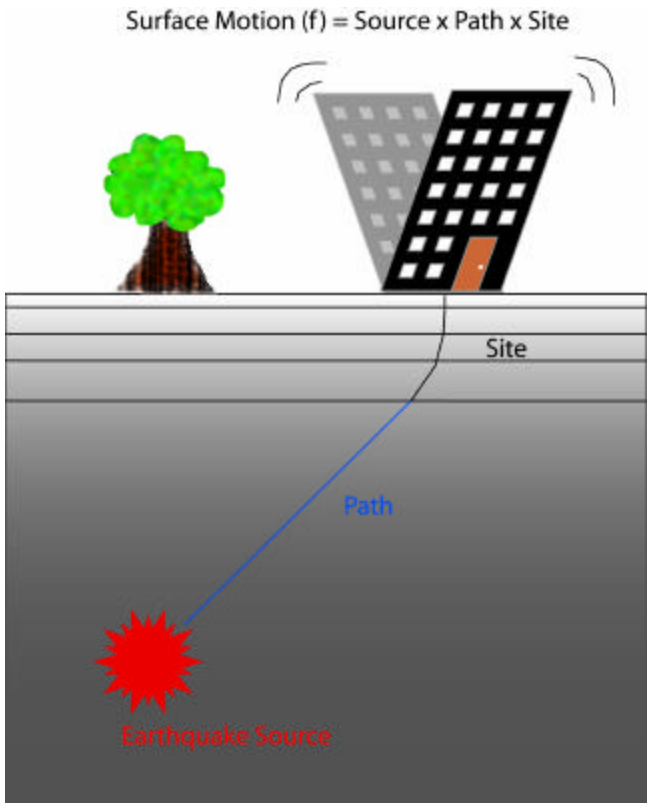

Figure 2.1: Schematic of parameters used to generate a surface motion in the frequency domain.

The separation of source, path, and site effects for earthquake ground motion parameters can be somewhat artificial. A strong site response can occur where a thin soil or sedimentary layer deposit overlies hard bedrock. In that case, the presence of the soil layer may represent the largest seismic velocity contrast present along the ray-path, and a well-defined site response is due to near-surface geologic conditions. However, sedimentary basins, such as the Los Angeles basin or thick deposits of sediments in areas such as the Atlantic, and Gulf coastal plains, may have gradual velocity contrasts extending over several kilometers of ray-path length that could be considered a path property rather than a property of the near surface. For these thick deposits, the response of the incoming seismic waves may involve complicated 2-D and 3-D phenomena due to wave scattering, focusing, and anelastic absorption (Olsen, 2000).

Snell's law governs the angle of refraction for seismic waves encountering a material boundary. Generally, seismic velocity will decrease as seismic waves approach the surface. When unconsolidated sediments are present, this change in velocity becomes so great near the surface that the incident rays will become almost normal to the surface.

In this case, the incoming earthquake motions will consist largely of horizontal shear waves. Generally, the horizontal component of the shear wave is greater in amplitude than the vertical component of the shear wave or the incident p wave. Also, most of the damage to buildings is from horizontal forces because structures are generally designed to withstand only vertical forces. For this analysis, all of the models will have sediments present above the crystalline bedrock, and, due to the large velocity changes in the near surface, vertical incidence of incoming seismic waves will be assumed.

The site effect of the near-surface materials will be modeled using a series of horizontal layers with varying density, thickness, damping, and shear wave velocity. These layers represent

soils, sedimentary deposits, and weathered rock and are assumed to be laterally continuous and uniform. An elastic half-space representing crystalline bedrock underlies the layered subsurface model and contains the earthquake source. The half-space is a continuum that has only one defined boundary: the interface with the layered model. The subsurface layers are assumed to be viscoelatic materials with an associated damping. An important aspect of the model is the fact that shear wave velocity and damping are treated as strain-dependent quantities. At high strain levels, soil layers exhibit nonlinear behavior such that damping and the shear modulus depend on the amount of strain applied (Kramer, 1996, p. 191)

Wave Equations for Linear Elastic and Viscoelastic Materials

Elastic materials with linear behavior

The following is a detailed discussion based on Schnabel, Lysmer, and Seed (1972) and Schnabel, Seed, Bolton, and Lysmer (1972 and 1973). Several of the ideas and equations are included in the publications.

The one-dimensional wave equation for a vertically propagating shear wave in an isotropic medium is:

$$r\frac{\partial^2 u}{\partial t^2} = \frac{\partial t}{\partial z}. \qquad 2.1$$

In equation 2.1, t is time, ρ is material density, u is displacement in the horizontal direction and τ is shear stress on a horizontal plane. The wave is assumed to propagate in the vertical z direction, assuming z is positive downward. For linear behavior, the shear stress is a linear function of the shear strain ?, where the constant of proportionality is the modulus of rigidity, G. For the one-dimensional elastic case, stress, strain, and displacement are related through:

$$t = Gg = G\frac{\partial u}{\partial z} \qquad 2.2$$

For an elastic material, the equation of motion is usually expressed as:

$$\frac{\partial^2 u}{\partial t^2} = \left(\frac{G}{r}\right)\frac{\partial^2 u}{\partial z^2} = c^2\frac{\partial^2 u}{\partial z^2}, \qquad 2.3$$

where c is the constant shear wave velocity:

$$c^2 = \frac{G}{r}. \qquad 2.4$$

Steady-state solutions of equation 2.3 are of the form

$$u(z,t) = Ae^{i(kz+wt)} + Be^{i(-kz+wt)}, \qquad 2.5$$

where ω is angular frequency and k = ω /c is known as the wave number. Equation 2.5 represents two harmonic waves traveling upward and downward in the material with amplitudes A and B, respectively.

Viscoelastic materials

Soils do not behave as linear elastic materials under strong shaking. Even at very small strain values, soils exhibit absorption of high frequency energy. This requires the use of another form of equation 2.1 to model the motion. A common approach to incorporate anelastic absorption of wave energy assumes viscoelastic behavior. Kramer (1996, p. 175) states, "For the purpose of viscoelastic wave propagation, soils are usually modeled as Kelvin-Voigt solids, (i.e., materials whose resistance to shearing deformation is the sum of an elastic part and a viscous part)." In this case, the shear stress depends on the rate of change of stain, as well as the strain magnitude. This dependence is given by:

$$t = Gg + h\left(\frac{\partial g}{\partial t}\right), \qquad 2.6$$

where ? is the *viscosity* of the material. Differentiation of equation 2.6, with respect to the spatial coordinate z, leads to:

$$\frac{\partial t}{\partial z} = G\frac{\partial g}{\partial z} + h\frac{\partial}{\partial z}\frac{\partial g}{\partial t}. \qquad 2.7$$

Substitution of 2.7 into the right hand side of equation 2.1 gives

$$r\frac{\partial^2 u}{\partial t^2} = G\frac{\partial g}{\partial z} + h\frac{\partial}{\partial z}\frac{\partial g}{\partial t}. \qquad 2.8$$

Equation 2.8 (above) is the one-dimensional wave equation for a viscoelastic material. It can be written entirely in terms of displacement, u, by noting that shear strain is, in general,

$$g = \frac{\partial u}{\partial z}. \qquad 2.9$$

Substitution of equation 2.9 into equation 2.8 and introducing index j to represent the material properties for a viscoelastic medium consisting of j =1,2,3….n horizontal layers leads to the following equation of motion for shear waves in each layer:

$$r_j\frac{\partial^2 u}{\partial t^2} = G_j\frac{\partial^2 u}{\partial z^2} + h_j\frac{\partial^3 u}{\partial z^2 \partial t}. \qquad 2.10$$

Following the development given by Schnabel, Lysmer and Seed (1972), a steady-state harmonic solution is assumed for each model layer with the following form:

$$u(z,t) = U(z)e^{iwt} \qquad 2.11$$

U(z) can be regarded as the Fourier coefficient of u(z,t), at a single frequency, ω, and represents the complex amplitude and phase of a harmonic displacement. Substitution of equation 2.11 into equation 2.10 leads to an ordinary differential equation:

$$rw^2U(z) = (G + iwh)\frac{d^2U(z)}{dz^2}. \qquad 2.12$$

The general solution of 2.12 for U(z), which we will hereafter interpret as representing the complex amplitudes of the harmonic components of motion in each layer is given by:

$$U_j(z) = E_j e^{ik_j z} + F_j e^{-ik_j z}. \qquad 2.13$$

In equation 2.13, the subscript j represents the particular layer. The complex wave number k is related to the material properties of the j'th layer through:

$$k_j{}^2 = \frac{r_j w^2}{G_j + iwh_j}. \qquad 2.14$$

Equations 2.11 and 2.13 give the solutions to the wave equation for harmonic displacements u(z,t) of frequency ω in the j'th layer:

$$u_j(z,t) = E_j e^{ik_j z + iwt} + F_j e^{-ik_j z + iwt} \qquad 2.15$$

The first term on the right hand side of equation 2.15 is a plane harmonic wave traveling in the negative z, upward, direction and the second term is the downward traveling plane harmonic wave. This solution is valid at any point in a given layer, where it is understood that u(z = 0,t) is motion at the top of a layer and u(z = h_j,t) is motion at the bottom of the layer, where h_j is the layer thickness. As shown in the following equations, amplitude coefficients, E_j and F_j, can be expressed in terms of E_{j+1} and F_{j+1} such that motions can be defined at all points within all layers, as described below.

Recursion relations

Conditions of continuity of displacement and stress across layer boundaries permit the development of recursive relationships relating motions at any depth in a given layer to motions within any other layer. Displacements at the top, z = 0, and bottom, z = h_j, of the j'th layer are, respectively:

$$u_j(0,t) = (E_j + F_j)e^{iwt}, \qquad 2.16$$

$$u_j(h_j,t) = (E_j e^{ik_j h_j} + F_j e^{-ik_j h_j})e^{iwt}. \qquad 2.17$$

Shear stress is given by substituting 2.9 into 2.6:

$$t_j(z,t) = G_j g + h_j \frac{\partial g}{\partial z} = G_j \frac{\partial u_j}{\partial z} + h_j \frac{\partial^2 u_j}{\partial z \partial t}. \qquad 2.18$$

Differentiation of 2.15 and substitution into 2.18 leads to:

$$t_j(z,t) = ik_j(G + ihw)\left[E_j e^{-ik_j z} - F_j e^{-ik_j z}\right]e^{iwt}. \qquad 2.19$$

Hence, shear stresses at the top and the bottom of the j'th layer are, respectively,

$$t_j(0,t) = ik_j(G + ihw)\left[E_j - F_j\right]e^{iwt}, \qquad 2.20$$

$$t_j(h_j,t) = ik_j(G + ihw)\left[E_j e^{-ik_j h_j} - F_j e^{-ik_j h_j}\right]e^{iwt}. \qquad 2.21$$

Displacements across all layer interfaces must be continuous. This condition is expressed by equating 2.16 and 2.17, where there are two layers shown with the indices j and j+1 that share an interface:

$$E_{j+1} + F_{j+1} = E_j e^{ik_j h_j} + F_j e^{-ik_j h_j}. \qquad 2.22$$

Also, stress must be continuous across all layer interfaces. Equating 2.20 and 2.21 for two different layers shown with indices j and j+1 leads to:

$$E_{j+1} - F_{j+1} = \frac{ik_j(G_j + ih_j w)}{ik_{j+1}(G_{j+1} ih_{j+1} w)}(E_j e^{ik_j h_j} - F_j e^{-ik_j h_j}). \qquad 2.23$$

To simplify notation, the complex shear modulus G* is introduced:

$$G_j^* = G_j + iwh_j \quad . \qquad 2.24$$

The damping ratio, β, of the material is related to viscosity by (Schnabel, Lysmer and Seed, 1972, p. 4):

$$wh = 2Gb \, . \qquad 2.25$$

Schnabel, Lysmer and Seed (1972) assume that G and β are essentially independent of frequency for soils and substitution of 2.25 in 2.24 leads to:

$$G_j^* = G_j(1 + i2b_j). \qquad 2.26$$

From 2.14, the complex wave number is defined as:

$$k_j^2 = \frac{r_j w^2}{G_j^*}. \qquad 2.27$$

Using equations 2.27 and 2.24, equation 2.23 is rewritten as:

$$E_{j+1} - F_{j+1} = a_j(E_j e^{ik_j h_j} - F_j e^{-ik_j h_j}), \qquad 2.28$$

where α_j is a complex impedance ratio defined by:

$$a_j = \left(\frac{r_j G_j^*}{r_{j+1} G_{j+1}^*} \right)^{1/2}. \qquad 2.29$$

The complex amplitudes of the up-going and down-going wave field in different layers are shown below. Adding 2.28 and 2.22 results in:

$$E_{j+1} = \frac{1}{2} E_j \left[\left(1 + a_j\right) e^{(ik_j h_j)} \right] + \frac{1}{2} F_j \left[\left(1 - a_j\right) e^{(-ik_j h_j)} \right]. \qquad 2.30$$

Subtraction of 2.28 from 2.22 leads to:

$$F_{j+1} = \frac{1}{2} E_j \left[\left(1 - a_j\right) e^{(ik_j h_j)} \right] + \frac{1}{2} F_j \left[\left(1 + a_j\right) e^{(-ik_j h_j)} \right]. \qquad 2.31$$

Equations 2.30 and 2.31 can be applied recursively to express amplitudes at any point in the model in terms of amplitudes at any other point.

Treatment of Site Response for Engineering Applications

Equation 2.13, in conjunction with 2.29 and the recursion relations 2.30 and 2.31 allows the development of transfer functions, which relate motions at any two locations in an Earth model. The model consists of n horizontal layers overlying a half-space, where the j = 1 layer represents the surface layer and the j = n layer represents the deepest layer adjacent to the half space. The half space is represented by the index j = n+1. The downward direction is represented by positive z and the upward direction will be represented by negative z. Figure 2.2 shows an illustration of a general Earth model.

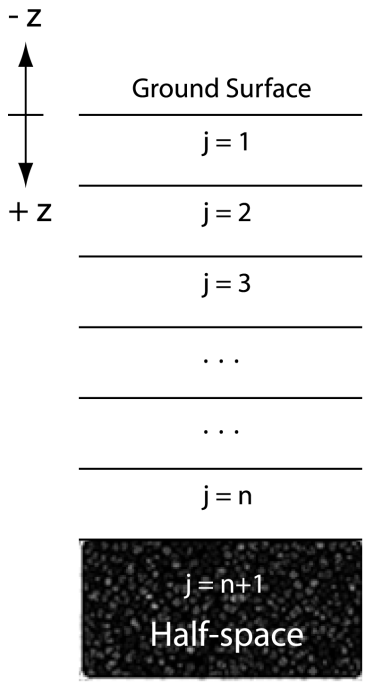

Figure 2.2: Schematic for generalized Earth model

At the top of the j = 1 layer, the Earth's free surface, the shear stress is zero. From Equation 2.20, substituting in z = 0 and j = 1 results in:

$$t_1(z=0,t) = ik_1 G^*(E_1 - F_1)e^{iwt} = 0. \qquad 2.32$$

Therefore, for the j =1 layer, the up-going and down-going Fourier coefficient amplitudes are equal, $E_1 = F_1$. For simplicity, setting $E_1 = F_1 = 1$ allows a recursive computation of E_j and F_j for all layer interfaces in the model and allows the ratio of motions to be defined in the frequency domain at any two points in the model. Beginning with the surface layer, j = 1, equations 2.30 and 2.31 are used to evaluate E_{j+1} and F_{j+1} at successive interfaces.

For example, assume that the ground motion is recorded on the free surface of a model consisting of n layers over a half-space. The material properties of the layers are known and the motions at the top of the half-space are required. The Fourier transform of the ground

displacement time series on the surface of the layered model is represented by $A_1(z=0,\omega)$ and the Fourier transform of the time series of the half-space motion is represented as $A_{n+1}(z=0,\omega)$. The motion at the two depths is related through a transfer function $T(\omega)$ as shown below. This function acts like a filter in the frequency domain and is the ratio of the Fourier coefficients:

$$T(w) = \frac{U_{n+1}(z=0,w)}{U_1(z=0,w)}. \qquad 2.33$$

A_{n+1}, the motion on the top of the half-space, in terms of the motion on the free surface, $A_1(z = 0)$, is:

$$A_{n+1}(z=0) = \frac{U_{n+1}(z=0)}{U_1(z=0)} A_1(z=0). \qquad 2.34$$

Using equation 2.13, the half-space and free-surface coefficients become, respectively,

$$U_{n+1}(z=0) = E_{n+1} + F_{n+1}, \qquad 2.35$$

and

$$U_1(z=0) = E_1 + F_1 = 2. \qquad 2.36$$

Equation 2.34 can be expanded to encompass any location in the Earth model. This generalization of equation 2.34 is shown below:

$$A_p(z) = \frac{U_p(z)}{U_q(z)} A_q(z) = \frac{E_p e^{ik_p z} + F_p e^{-ik_p z}}{E_q e^{ik_q z} + F_q e^{-ik_q z}} A_q(z), \qquad 2.37$$

where p = 1,2,….n+1 and q = 1,2,….n+1 are the indices referring to differing locations in the Earth model for n layers overlying a half space and z refers to depth within a given layer. In 2.37, it is assumed that displacement $A_q(z)$ is known and $A_p(z)$ is determined with knowledge of the layer thicknesses and material properties.

The most frequent engineering application involves calculation of motions at various points in an Earth model, given recorded motions on an outcrop of the half-space material. This problem will be treated in the following chapters. In this study, a half-space outcrop motion, represented by A^{o}_{n+1}, will be assumed as the input motion. The input motion will be multiplied by an appropriate transfer function to produce the surface motion. The desired output will be the free surface motion on the layered Earth structure. In the notation of equation 2.37, the motion at the local depth z within any layer j, given motions recorded on a half-space outcrop is given by:

$$A_j(z) = \frac{U_j(z)}{U_{n+1}} A^o_{n+1} = \frac{E_j e^{ik_j z} + F_j e^{-ik_j z}}{2E_{n+1}} A^o_{n+1}. \qquad 2.38$$

In this case, assuming that $E_1 = F_1 = 1$, the motion on the free surface of the j = 1 layer is given by:

$$A_1(z = o) = \frac{2}{2E_{n+1}} A^o_{n+1}. \qquad 2.39$$

Strains at any point in the model may be determined by:

$$g_j(z) = \frac{\partial A_j(z)}{\partial z} \quad . \qquad 2.40$$

For the case wherein the half-space outcrop motion is known and used to calculate motions at other points in the model, equations 2.38 and 2.40 lead to:

$$g_j(z) = \frac{ik_j(E_j e^{ik_j z} - F_j e^{-ik_j z})}{2E_{n+1}} A^o_{n+1}. \qquad 2.41$$

Figure 2.3 shows a visualization of using the transfer functions to calculate the free surface motions of the Earth model:

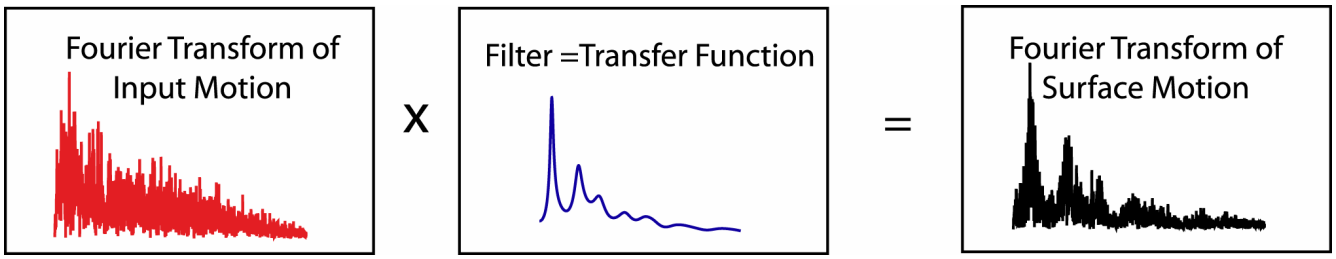

Figure 2.3: Demonstration of how the surface motions are calculated using transfer functions

After the surface motions are calculated, an inverse Fourier transform is used to obtain the resultant motion in the time domain and produce a surface motion time series.

Non-Linear Behavior and the SHAKE Algorithm

In addition to anelastic absorption or viscoelastic behavior, soils may exhibit strain dependent or non-linear behavior. In effect, the complex shear modulus G* is strain dependent under strong earthquake ground motions. The equations of motion above assume that G* is independent of strain and the material exhibits linear behavior. Schnabel, Seed, Bolton and Lysmer, 1972 and 1973 introduced an approximate solution to the non-linear problem using an iterative application of the linear viscoelastic solution detailed above. A well-known computer program that implements this algorithm is called SHAKE (Schnabel, Seed, Bolton ,and Lysmer, 1972 and 1973; Schnabel, Lysmer ,and Seed, 1972) and it has been used by the engineering community for many years. The method is often referred to as an "equivalent linear" approach, and is viable for certain circumstances. However it is more accurately described as a linear approximation. This equivalent linear approach assumes that the near-surface materials are undergoing symmetric cyclic forces with small strains and that permanent deformation of the near-surface model does not occur (Kramer 1996, p. 231).

The equivalent linear modeling approach refers to how the near-surface material mechanical behavior is described. Empirical data show that energy dissipation occurs at low

strain levels causing the stress-strain graph to be elliptical or hysteretic in shape (Kramer 1996, p. 238) as shown in Figure 2.4a.

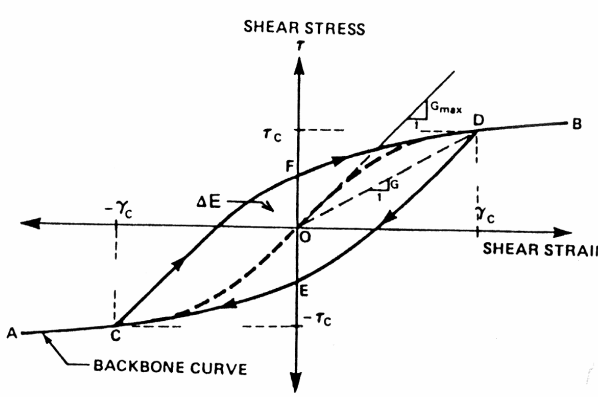

Figure 2.4a: Hysteresis loop for soil showing the stress changing with different shear strain (from Vucetic and Dobry, 1991, used with permision of publisher, ASCE)

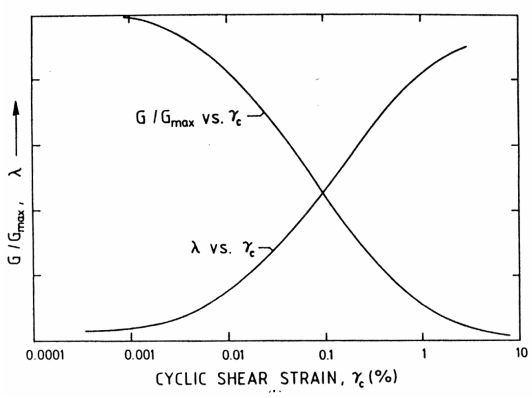

Figure 2.4b: Simplified normalized shear modulus and damping versus shear strain curves (from Vucetic and Dobry, 1991, used with permission of publisher, ASCE)

As soils are subjected to several cycles of stress, the stress-strain diagram for the soil will be a complicated path made up of a number of continuous hysteresis loops. The path will trend towards the horizontal shear strain axis. This complex stress-strain path diagrams the mechanical parameters, shear modulus ,and damping of the soil.

The linearized approach assumes an average shear modulus value of the path of the hysteretic loop called G_{sec} and the G_{sec} value will decrease as the shear strain increases. G_{sec} is defined as the ratio of critical shear stress to critical shear strain and lies at the point where the hysteresis loop changes slope, shown as point D in figure 2.4a:

$$G_{\sec} = \frac{t_c}{g_c}. \qquad 2.41.$$

The shear modulus value used in this equivalent approximation is a ratio of G_{sec} to G_{max} and is referred to as G, the normalized shear modulus. G_{max} is the maximum shear modulus value and

is the equal to G_{sec} at low shear strain values. An example of a normalized shear modulus versus strain curve is shown in figure 2.4b.

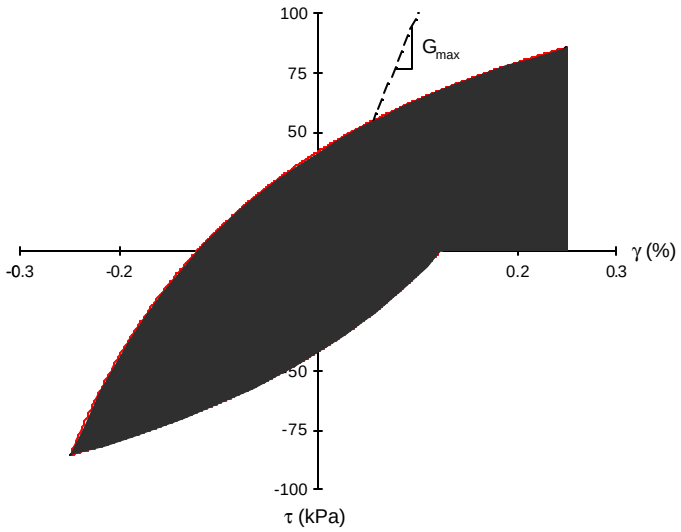

Figure 2.5: Hysteresis diagram for one cycle of stress that shows the portions of the curve used to calculate the damping ratio (Olgun 2004)

The damping ratio, ß, is also dependent upon the hysteretic behavior of the soil and the amount of energy absorption. It is generally defined as:

$$b = \frac{1}{4p} \cdot \frac{\Delta W}{W}, \qquad 2.42$$

where ?W is the area of the triangle, shown in orange in figure 2.5, that is bordered by the line tangent to the G_{sec} point and the intersecting portions of the axes. W, shaded in blue in figure 2.5, represents the area of the hysteresis loop and is related to the amount of energy dissipated. Several of these diagrams, generated from empirical tests, will combine to create a critical damping ratio versus shear strain curve as shown in figure 2.4b and this curve will be used in the linear approximation.

The equivalent linear algorithm requires normalized shear modulus and damping versus strain curves, velocity, density, and thickness for each layer and an input acceleration time series for the outcropping half-space. The normalized shear modulus and damping versus strain curves are for a range of strain. These curves are dependent upon the type of material and can be different for each model layer. They can be generated for the specific site with geotechnical laboratory data. However, the following generalized shear modulus and damping models are the most commonly used: Assimaki et al. (2000) for deep materials, Vucetic and Dobry (1991) for fine materials, and Ishibashi and Zhang (1993) for sands. Figure 2.6 shows examples of normalized shear modulus and damping versus strain for the aforementioned models.

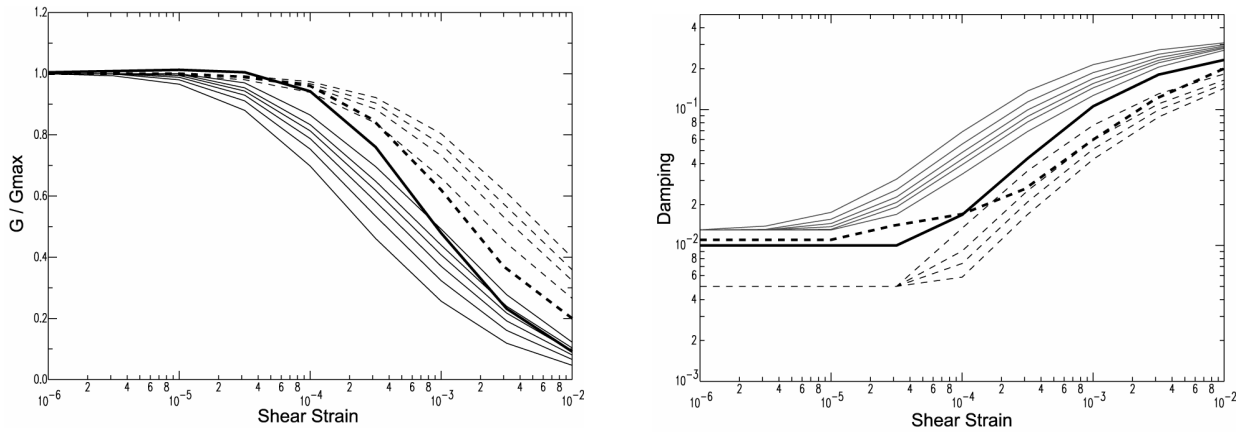

Figure 2.6: An example Normalized Shear modulus and material damping curves as a function of shear strain. The solid lines are for sands (from Ishibashi and Zhang, 1993). The thin dashed lines are for deep materials (Assimaki et al., 2000, 2001).

An approximation used by the equivalent linear approach involves "effective strain". The algorithm uses a constant measure of strain for the entire earthquake time series in any given layer. This effective strain is less than the maximum strain during the earthquake. The effective strain is the peak value of strain for each layer multiplied by a magnitude dependent constant. As a result, a single value for normalized shear modulus and damping is used throughout the

earthquake event in each layer. Both of these assumptions are approximations. However, this approach is computationally inexpensive and is a good approximation for small strains. Other approaches that describe the soil's stress-strain behavior more accurately require additional information on material behavior and are computationally extensive.

Comparisons by Hartzell et al. (2004) of the equivalent linear algorithm with other equivalent linear frequency dependent and nonlinear algorithms indicate that the equivalent linear algorithm produced approximately the same results for small strain levels. Over damping from the equivalent linear algorithm was observed at motion levels beyond 0.4 g and for softer sites.

The equivalent linear algorithm is outlined in figure 2.7. After the complex impedance ratio and wave number are calculated, the up-going and down-going amplitude coefficients are calculated along with the transfer functions for the motions and strains in the middle of each layer. The motions and strains are then calculated by multiplying the Fourier transform of the input motion with the appropriate transfer function and performing an inverse Fourier transform to express the motions and strain in the time domain. The effective strain is calculated for each layer and used to determine the updated normalized shear modulus and damping values. The previous normalized shear modulus and damping values are compared to the new values. If the difference is zero, then the algorithm has reached a stable answer. However, if the difference is large, the normalized shear modulus and damping value are updated and the process is repeated. If strains are small in all model layers, approximately 0.03 or less, the algorithm will usually reach stability within 5 to 10 iterations. If larger strains occur in one or more of the layers, the algorithm may not stabilize and strain-compatible modulus and damping cannot be determined.

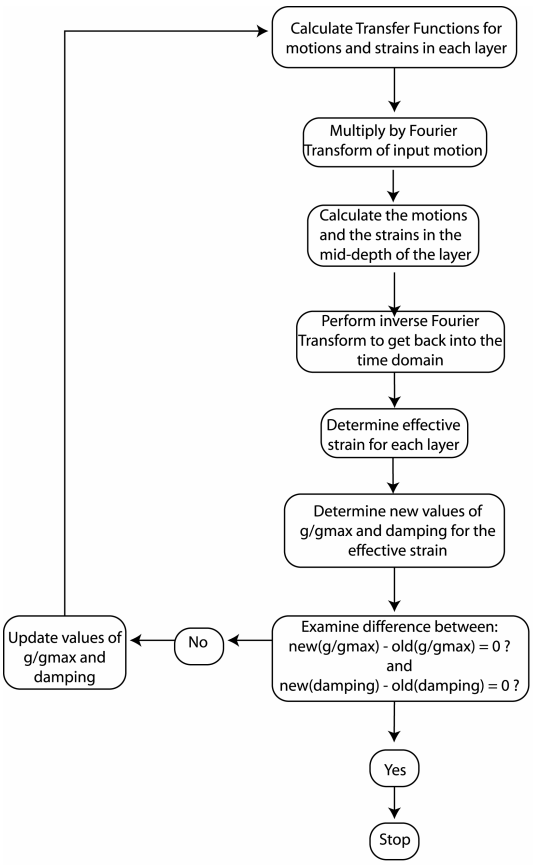

Figure 2.7: Overview of the equivalent linear algorithm from Schnabel, Lysmer and Seed (1972) SHAKE and the current version by Dr. Chapman

Many revisions have been made to the original SHAKE computer program. Each change has improved upon its versatility; although, the most recent versions remain limited in the number of layers and strain dependent behavior models that can be applied. This is a major shortcoming when depth dependent shear modulus and damping models are required.

The equivalent linear algorithm implemented in this study used a program developed by Dr. Martin Chapman. The program does not limit the number of materials or layers for the subsurface model and offers several improvements with regard to model input and output of results.

Chapter 3: Generating Input Motions

This study follows current practice in which scenario earthquakes based on probabilistic seismic hazard analysis are used to define time series for site response analysis. A recent example of this approach is a study by the Tennessee Valley Authority (Munsey, 2004). This study uses the results of the U.S. Geological Survey national seismic hazard mapping project to define scenario earthquakes, earthquake magnitudes, and the source to site distances for site response analysis.

The national seismic hazard maps are a statistical representation of the seismic hazard across the United States. The first version was published by Algermissen and Perkins (1976) and has been updated and revised several times in ensuing years. A major procedural change occurred with the 1996 version of the maps (Frankel, 1995 and Frankel et al., 1996). Frankel (1995) describes the procedures used in previous versions of the U.S. Geological Survey national hazard maps. The Frankel et al. (1996) maps have been incorporated as reference maps in the 1997 version of the National Earthquake Hazards Reduction Program (NEHRP) Provisions (FEMA, 1997). The national seismic hazard maps were updated in 2002 and this study will use these results (Frankel et al. 2002).

The national seismic hazard maps are made using a method called probabilistic seismic hazard analysis, or PSHA, which estimates the probability of exceedance of different levels of ground motion intensity at a given location. This method was originally developed by Cornell (1968). The fundamental assumption underlying PSHA is that earthquakes follow a stationary Poisson process, which assumes the events are independent of each other (Ang and Tang, 1975, p. 114). This is approximately valid for earthquake catalogs that have been "declustered", i.e., catalogs in which all dependent earthquakes, aftershocks and foreshocks, have been deleted. The process is defined by a single parameter: λ, the mean time rate of events that constitute the process.

The Poisson process is the simplest stochastic process that can be applied to PSHA. In general, a Poisson process is defined using the Poisson probability distribution:

$$P(X_t = x) = \frac{(\lambda t)^x}{x!} e^{-\lambda t}, \quad \text{for x = 0, 1, 2,....} \qquad (3.1)$$

In equation 3.1, $P(X_t = x)$ represents the probability of occurrence of exactly x "events" in time interval t. This probability is completely defined by knowledge of λ, the mean rate, discussed below. Equation 3.1 is simplified by examining the probability of at least one event occurring in time interval t:

$$P(X_t > 0) = 1 - P(X_t = 0) = 1 - e^{-\lambda t}. \qquad (3.2)$$

In PSHA, λ is usually an "expectation" representing the expected rate of at least one exceedance of a specified ground motion level at a specific location due to occurrence of earthquakes within a specified magnitude and distance range. The PSHA treats magnitude and distance as random variables. The expected rate, λ, of exceeding a specified ground motion, x, can be represented by:

$$\lambda = E(X > x) = \nu \int_{M_o}^{M_{\max}} \int_{R_o}^{R_{\max}} \int_{\varepsilon_o}^{\varepsilon_{\max}} f_m(m) \cdot f_r(r \mid m) \cdot f_\varepsilon(\varepsilon) \cdot H(\psi(m,r,\varepsilon) - x) \cdot d\varepsilon \cdot dr \cdot dm \quad 3.3$$

where m is magnitude, r is distance from epicenter to site, ε is the random variable representing the variability in the ground motion prediction model, ν is the rate of earthquakes with magnitudes greater than a minimum magnitude M_0, the probability density function of the earthquake magnitude is $f_m(m)$, the probability density function of the earthquake epicenter to site distances, conditional on magnitude, is $f_r(r|m)$ and the probability density function of ε is $f_\varepsilon(\varepsilon)$. The argument of the Heaviside function, H, is the difference between a median predicted ground motion value and a specified ground motion value, x.

The variable ψ, in equation 3.3, represents a ground motion prediction model that may represent any one of several motion parameters, e.g. peak ground acceleration, peak ground velocity, or oscillator spectral response. This model may be based on empirical earthquake data from various tectonic settings or upon theoretical models. As shown in equation 3.3, motion prediction depends on magnitude, distance from the epicenter to the site, and includes an error term. The geologic setting of the site and scenario earthquake parameters should be consistent with the hazard model parameters as much as possible. There are several different ground motion prediction models for the intraplate tectonic setting for the east coast and they generally assume bedrock outcrop conditions. The prediction models used for the 2002 national seismic hazard maps (Frankel et al., 2002) include: Toro et al. (1997), Frankel et al. (1996), Atkinson and Boore (1995), Sommerville et al. (2001) and Campbell (2003).

The national seismic hazard maps are based on the National Earthquake Hazards Reduction Program or NEHRP (1997) site classification scheme and correspond to motions on sites classified as B-C material. This site condition is based on an average shear wave velocity of 760 m/s in the top 30 meters (Martin and Dobry 1994). This assumption complicates the use of the national seismic hazard maps site in cases where the generic site condition does not exist. This issue will be addressed in Chapter 5.

In equation 3.3, the rate of earthquakes,ν, and the probability density function of magnitude depends upon the history of earthquakes surrounding the site. The historical earthquake catalog is often used in PSHA to develop a seismicity recurrence relation in the form of the Gutenberg-Richter relationship (Gutenberg and Richter, 1954):

$$LogN = a - bM \quad . \qquad (3.4)$$

For equation 3.4, N is the number of earthquakes per unit time larger than magnitude M. A truncated form of equation 3.4 is often used for PSHA. Small magnitude events are not of concern for PSHA because they do not damage buildings. Therefore a minimum magnitude, M_0, of concern is defined and typical values are in the range of $M_0 = 4.5$ to $M_0 = 5.0$. Any given earthquake source will have a maximum magnitude, M_{max}, constrained by tectonic setting. The intercept a, in equation 3.4, depends on the strain rate in the area of concern. It reflects the rate of earthquakes per unit area and therefore has large geographic variability. The b value, slope of equation 3.4, is nearly constant worldwide with a value of approximately 1.0. The Gutenberg-Richter relationship implies that earthquakes have an exponential magnitude probability distribution in which small magnitude events are much more frequent than large magnitude events. As used in PSHA, the parameter ν, in equation 3.3, is the rate of earthquakes with magnitude greater than minimum magnitude M_0 and less than maximum magnitude $M_{max,}$ hence:

$$\nu = 10^{a-bM_0} - 10^{a-bM_{\max}}. \qquad (3.5)$$

The PSHA model incorporates the upper and lower magnitude bounds, M_{max} and M_0. Therefore, the magnitude probability density distribution is truncated and has the following form:

$$f_m(m) = 0, \quad m < m_0$$
$$f_m(m) = \frac{b' e^{-b'm}}{e^{-b'm_0} - e^{-b'm_{\max}}}, \quad m_0 \le m \le m_{\max} \qquad (3.6)$$
$$f_m(m) = 0, \quad m > m_{\max}$$

where b' = bln(10) = b(2.303).

There are other representations of the seismic recurrence that do not follow the Gutenberg-Richter relationship. Frankel (1995) incorporates a characteristic earthquake model, for source areas like Charleston, SC, that exhibit geological evidence of recurring large magnitude earthquakes. For this scenario, a different probability density distribution for magnitude is applied:

$$f_m(m) = \delta(m - m_{char}),\ m_0 \le m \le m_{\max}. \qquad (3.6)$$

Equation 3.6 contains a delta function which represents the occurrence of a repeating or characteristic earthquake of a specific magnitude, M_{char}, in a given source.

The conditional probability density distribution for distance to earthquake sources, $f_r(r|m)$ in equation 3.3, depends on the geometry and distance of the source and the site, as well as the earthquake magnitude. Typical representations of the source include a point, line, or area with a specified orientation or shape.

The $f_\varepsilon(\varepsilon)$ or the probability density distribution for random error in equation 3.3 is defined as a normal distribution on logarithms of peak ground motions or damped oscillator response. Because most ground motion prediction models are derived by regression analysis, the standard deviation of the $f_\varepsilon(\varepsilon)$is often assumed to be equal to the regression standard error of estimate.

Equation 3.3 is a general expression for a single earthquake source. Usually, there are multiple possible sources near the site and the total seismic hazard is the sum of all the possible earthquake sources.

A uniform hazard spectrum, UHS, is a response spectrum wherein all ordinate values have the same hazard or probability of exceedence. This spectrum has contributions from all of the defined sources used in the PSHA. The UHS may be used as a target design spectrum; however, the UHS assumes that spectral ordinates at different frequencies are statistically independent and it does not generally represent the spectrum of a specific scenario earthquake. The exception is in cases where the seismic hazard is dominated by a specific scenario earthquake, (i.e. where a characteristic earthquake at a well defined location dominates the hazard). In this case, the shape of the uniform hazard spectrum will approximately match that of the scenario earthquake.

Important information for establishing a scenario earthquake (or earthquakes) can be extracted by deaggregating the PSHA for a specified probability of exceedance (Chapman, 1995; McGuire, 1995). Deaggregation amounts to plotting the integrand of equation 3.3. This plot is typically constructed as a three dimensional graph that shows the percentage of hazard contribution over the range of specified magnitudes and distances for the study. The deaggregation is calculated for a specified hazard level or probability of exceedance and is used as a guide in defining scenario earthquakes for design purposes (e.g. Chapman 1995, McGuire 1995). These graphs are available from the USGS for all locations in the United States. An example of a deaggregation plot is shown below in figure 3.1. The colors correspond to different levels of error or ε in the ground motion attenuation models.

For the study site, Columbia, South Carolina, one seismic event controls the seismic hazard. The seismic event is a magnitude 7.3 event at 123 kilometers distance that represents the characteristic Charleston seismic source. Chapter 5 discusses using this scenario event in modeling the site response for the study area.

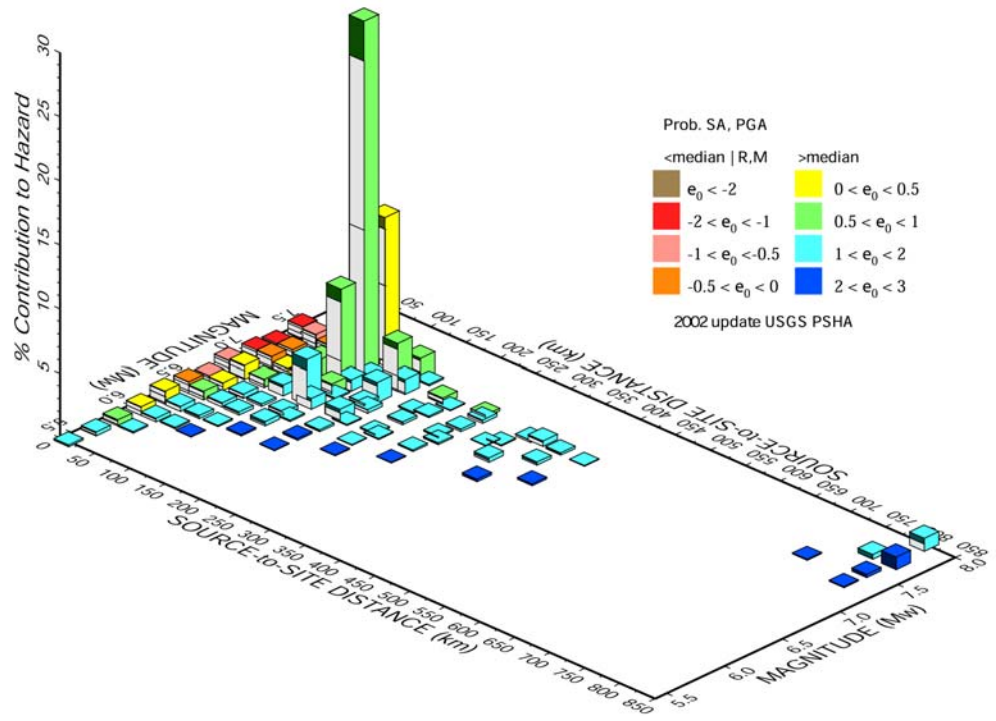

Figure 3.1: An example PSHA deaggregation plot from USGS National Seismic Hazard Mapping Project
website: http://eqint.cr.usgs.gov/eq/html/deaggint2002.html

Input Motions

The largest historical seismic events in the eastern United States include the 1811-1812 New Madrid and 1886 Charleston events. These events occurred prior to seismic instrumentation on this continent. Due to the lack of an adequate number of recordings from large magnitude (M > 5) earthquakes in the eastern United States, the input motions used for this analysis are generated synthetically using the stochastic model.

The stochastic model has been used for many years to estimate strong motions for sites in Eastern North America. It has its roots in the work of Hanks and McGuire (1981) and has seen continual development (e.g. Boore, 1983; Boore and Atkinson, 1987; Atkinson and Boore, 1995; Boore, 1996). The stochastic model represents high-frequency ground motion from a point source model and represents specific wave propagation effects that are unique to eastern North America.

Stochastic Model

As discussed in Chapter 2, shear waves are the primary concern for earthquake engineering. The stochastic model focuses on representing the high frequency shear wave radiation from earthquakes in the far field. The Fourier amplitude spectrum of ground acceleration in the stochastic model has the following form:

$$a_s(\omega) = |S(\omega)| \cdot |P(\omega)| \cdot |\Psi(\omega)|, \qquad (3.7)$$

where S(ω) is a source function, P(ω) is a path function and Ψ(ω) is a stochastic process. The point source is assumed to have a "Brune" or ω^{-2} spectrum (Brune 1970, 1971):

$$S(\omega) = \frac{R_{\theta\varphi}}{4\pi\rho V_s^{\,3}} \cdot \frac{M_o}{r} \cdot \frac{\omega^2}{1+(\frac{\omega}{\omega_c})^2}, \qquad (3.8)$$

where $R_{\theta\varphi}$ is the average radiation pattern for shear waves, ρ is the density, V_s is the shear wave velocity, M_o is the static seismic moment, r is the distance from the source, ω is angular frequency and ω_c, equal to 2 π f_c, is the corner frequency of the source spectrum. The geometric spreading is represented by the 1/r variable. The corner frequency, f_c, is a function of shear wave velocity, V_s, static seismic moment, M_o, and earthquake stress drop, Δσ (Boore 1983):

$$f_c = 4.9x10^6 V_s \left(\frac{\Delta\sigma}{M_o}\right)^{\frac{1}{3}}. \qquad (3.9)$$

The path factor shown in equation 3.10, below, contains a free surface effect, FS, and an exponential attenuation factor that is dependent upon the frequency, distance from the fault, r, shear wave velocity and Q, commonly called the quality factor.

$$P(\omega) = FS \cdot e^{-\omega r / 2QV_s}. \qquad (3.10)$$

The path, as defined in chapter 2, extends from the earthquake source to the near surface and represents propagation in crystalline or metamorphic rock with velocities approximately 3.5 kilometers per second. This high shear wave velocity crystalline or metamorphic rock will have some anelastic absorption of the seismic energy traveling through it. The exponential term exponent in 3.10 takes into account the anelastic absorption in the path effect, defined by Q which is related to the inverse of the damping ratio of a material.

The random variable in equation 3.7, $\Psi(\omega)$, is usually represented by Gaussian white noise; however, this is not a necessary assumption. For this study, Ψ is a stationary process, in the time domain, meaning that this function will have a constant mean and a standard deviation that is a nonzero constant throughout time. The Gaussian white noise will be modified by using a shaping window so that it will resemble the envelope of a squared acceleration time series. Boore (1983) gives the following suggestion for an appropriate shaping window:

$$w(t) = at^b e^{-ct} H(t), \qquad 3.12$$

where the values of the constants, a, b, and c, used in this study, are defined by Boore (1983) and H(t) is the Heaviside function. The source duration will be dependent on the corner frequency (e.g. Hanks and McGuire 1981):

$$T_d = \frac{1}{f_c}. \qquad 3.13$$

Scaling time series

Recall that the probability density function for ε is a log normal distribution and the function has non-zero values that go to positive infinity. This function can influence the PSHA a great deal by incorporating the large variability of the ground motion prediction model. The hazard level of interest in this study is 2% probability of exceedence in 50 years of exposure. This corresponds to

an annual exceedence rate of 4.04 x 10^{-4} or a mean return period of 2475 years. [1] This return period is substantially longer than the mean return period of the characteristic earthquake in the coastal plain South Carolina sources used by Frankel et al. (1996 and 2002) in developing the national seismic hazard maps. Hence, the ground motions corresponding to the 2475 year hazard exceed the median predicted motions of the characteristic events. The synthetic stochastic time series representing median estimates of motion for the scenario earthquake must be scaled upward to match the target 2475 year uniform hazard spectrum.

For this study, the synthetic time history was scaled to match the entire uniform hazard spectrum for the 2500 year event, because the seismic hazard is dominated by the chosen scenario earthquake (moment magnitude 7.3 at 123 km distance). The uniform hazard spectra for the locations examined have one dominant contributor to hazard.

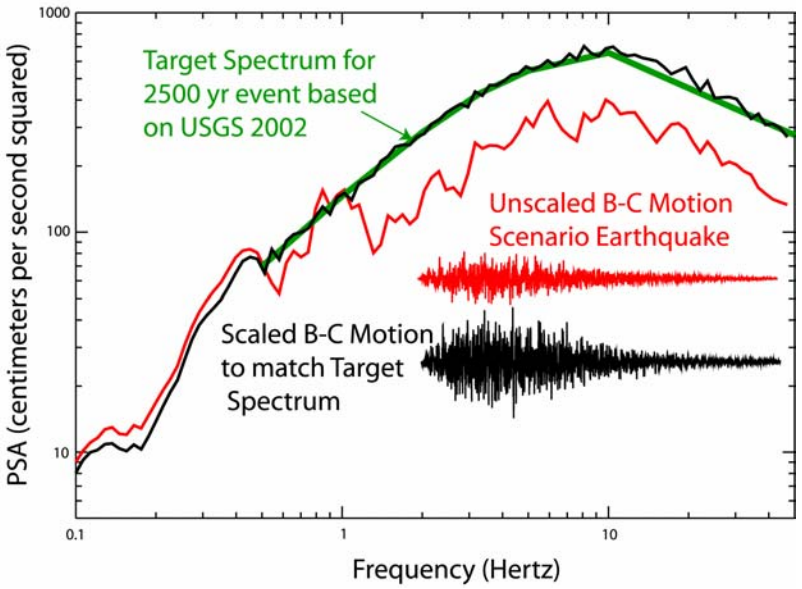

Figure 3.2: An example of scaling synthetic input motions to a target spectrum, shown in green. The scaled motion is shown in black

[1] $P = 1 - e^{-\lambda t}$, where P is probability of exceedance, λ is the mean rate of exceedance and t is the exposure interval. The mean return period is defined as λ^{-1}. For P = 0.02, t = 50 years, λ^{-1} equals 2475.

Chapter 4: International Building Code

The concept of building standards dates back to 1686 B.C. with the Code of Hammurabi (Wikipedia, 2004). Building codes typically did not address seismic hazards until large magnitude earthquakes impacted established cities such as the 1906 San Francisco earthquake. The general philosophy of seismic design in building codes is to protect life safety and withstand collapse from a strong earthquake (Hamburger and Kircher, 2000). Structures that survive an earthquake, and are built to code, may suffer extensive damage and be unusable.

The International Building Code, or IBC, is a publication from the International Code Council, ICC, which includes three well-known building code agencies: Building Officials and Code Administrators International, Inc., BOCA, International Conference of Building Officials, ICBO, and Southern Building Code Congress International, Inc., SBCCI (ICC 2004). A majority of the United States has adopted the International Building Code, IBC 2000. IBC 2000 is a model construction code (ICC 2004) that contains a seismic code that uses a modified version of the 1996 national seismic hazard maps to make design response spectra for structures.

There were many other building codes prior to the development of IBC 2000 that were region specific and each organization produced their own code. For example, the western United States had a primary building code, Uniform Building Code or UBC, which contained a seismic code specific to the frequent seismic activity in the region. The eastern United States generally used the BOCA code, which contained a very general seismic code statement.

In 1977, the National Earthquake Hazards Reduction Program (NEHRP) was created from public law 95-124 and revised in 1990 with public law 101-614. The main purpose of NEHRP is to reduce earthquake risk. NEHRP is made up of four federal agencies: Federal Emergency Management Agency (FEMA), the lead agency, National Institutes of Standards and Technology (NIST), National Science Foundation (NSF), and United States Geological Survey (USGS) (FEMA, 2004). FEMA publishes the *NEHRP Provisions* every three years showing the latest research and observational data in earthquake hazards and performance based design.

In 1993, the American Society of Civil Engineers adopted the 1991 NEHRP Provisions in their ASCE-7 publication. Widespread acceptance of the NEHRP Provisions was facilitated by the federal executive orders from 1990 and 1994, 12699 and 12941 respectively, that required federal buildings to comply with the NEHRP Provisions (FEMA 2004). Accordingly, BOCA and SBCCI adopted the ASCE 7 standards (Hamburger and Kircher 2000).

A significant step was taken with regard to seismic hazard nationwide when the 1997 version of the NEHRP Provisions adopted the 1996 National Seismic Hazard maps (Frankel et al 1996). South Carolina adopted the IBC 2000 in July 2000 (Lindberg and Associates), which incorporates the 1997 NEHRP Provisions. Hence, for the study area, the IBC 2000 code and the U. S. National Seismic Hazard maps form the basic design guidelines. To anticipate future developments in the IBC code, our ground motion estimates are based on the most recent version of the U.S. Geological Survey national seismic hazard maps (Frankel et al., 2002).

Developing IBC 2000 Design Response Spectrum

To develop the design spectra using the IBC design procedures, the site classification and spectral accelerations for two periods are required (IBC, 2000). The determination of the site classification is discussed below. The maps contained in the IBC 2000 are based upon the 1996 USGS National Seismic Hazard Maps. The IBC 2000 maps are approximately the same values as shown in Frankel et al. 1996 for the eastern United States. The IBC (2000) code specifies that the spectral accelerations (SA) for the location, in percent g, at 0.2 and 1.0 second period are used.

The site class is based upon the behavior of subsurface materials and can be determined by geotechnical investigations, including measurements of shear wave velocity, average standard penetration resistance and average undrained shear strength. The analysis in this study uses the average shear wave velocity for site classification.

The average shear wave velocity should be determined using individual layer thickness divided by the vertical shear wave travel time through the layer. The subsurface velocity information is usually provided in shear wave velocity values over a repeated interval and should be recalculated to get the total distance using the time traveled in the complete sampled interval. IBC only requires information for the top 30 meters; therefore, the total distance should not exceed 30 meters. The following formula is provided in the building code for summing the shear wave velocity over the individual layers:

$$\overline{V_s} = \frac{\sum_{i=1}^{n} d_i}{\sum_{i=1}^{n} \frac{d_i}{v_{si}}}. \qquad 4.1$$

The calculation of the average shear wave velocity, $\overline{V_s}$, includes the thickness of the

individual soil layer, d_i, and the shear wave velocity for the individual layer is v_{si}.

IBC states that if there is not sufficient subsurface information available, the site should be classified as site class D or lower. See table 4.1 for the complete listing of classifications adapted from the IBC 2000 classification table.

Table 4.1 Site Classification

Site Class	Average Soil Shear Wave Velocity, Vs (m/s)
A	Vs > 1524
B	1524 = Vs > 766
C	766 = Vs > 366
D	366 = Vs >183
E	Vs < 183

The site coefficients are found using the spectral acceleration in percent g from the 0.2 and 1.0 second period maps and the site classification from table 4.1.

TABLE 1615.1.2(1)
VALUES OF SITE COEFFICIENT F_a AS A FUNCTION OF SITE CLASS AND MAPPED SPECTRAL RESPONSE ACCELERATION AT SHORT PERIODS (S_S)[a]

SITE CLASS	MAPPED SPECTRAL RESPONSE ACCELERATION AT SHORT PERIODS				
	$S_S \le 0.25$	$S_S = 0.50$	$S_S = 0.75$	$S_S = 1.00$	$S_S \ge 1.25$
A	0.8	0.8	0.8	0.8	0.8
B	1.0	1.0	1.0	1.0	1.0
C	1.2	1.2	1.1	1.0	1.0
D	1.6	1.4	1.2	1.1	1.0
E	2.5	1.7	1.2	0.9	Note b
F	Note b	Note b	Note b	Note b	Note b

a. Use straight line interpolation for intermediate values of mapped spectral acceleration at short period, S_S.
b. Site-specific geotechnical investigation and dynamic site response analyses shall be performed to determine appropriate values.

TABLE 1615.1.2(2)
VALUES OF SITE COEFFICIENT F_v AS A FUNCTION OF SITE CLASS AND MAPPED SPECTRAL RESPONSE ACCELERATION AT 1 SECOND PERIOD (S_1)[a]

SITE CLASS	MAPPED SPECTRAL RESPONSE ACCELERATION AT 1 SECOND PERIOD				
	$S_1 \le 0.1$	$S_1 = 0.2$	$S_1 = 0.3$	$S_1 = 0.4$	$S_1 \ge 0.5$
A	0.8	0.8	0.8	0.8	0.8
B	1.0	1.0	1.0	1.0	1.0
C	1.7	1.6	1.5	1.4	1.3
D	2.4	2.0	1.8	1.6	1.5
E	3.5	3.2	2.8	2.4	Note b
F	Note b	Note b	Note b	Note b	Note b

a. Use straight line interpolation for intermediate values of mapped spectral acceleration at 1-second period, S_1.
b. Site-specific geotechnical investigation and dynamic site response analyses shall be performed to determine appropriate values.

Figure 4.1: Site Coefficient table for design response spectra. 2000 International Building Code. Copyright 2000. Falls Church, Virginia: International Code Council, Inc. Reproduced with permission. All rights reserved.

The site coefficients and spectral acceleration values from the IBC maps are used to calculate

the maximum considered earthquake spectral response acceleration. The equations below show the maximum considered earthquake spectral response accelerations for both the 0.2 period, S_{ms}, and one second period, S_{m1}, respectively:

$$S_{ms} = F_a \cdot S_s \qquad 4.2$$

and

$$S_{m1} = F_v \cdot S_1, \qquad 4.3$$

where F_a is the site coefficient for short period, S_s represents the spectral accelerations for short periods from the IBC map, the site coefficient for 1 second period is Fv and S_1 is the spectral accelerations for 1 second period, also from the IBC 2000 map.

The design spectral response acceleration is calculated using the maximum considered earthquake spectral response acceleration times two-thirds. See formula below:

$$S_{DS} = \frac{2}{3} S_{ms} \qquad 4.4$$

and

$$S_{D1} = \frac{2}{3} S_{m1} \qquad 4.5$$

Generating Design Spectra

The acceleration design spectra are defined as follows for a range of fundamental periods, T:

$$S_a = 0.6 \frac{S_{DS}}{T_o} * T + 0.4 * S_{DS}, \quad T \le T_o, \qquad 4.6$$

$$S_a = S_{DS}, \quad T_o < T \le T_s, \qquad 4.7$$

$$S_a = \frac{S_{D1}}{T}, \; T > T_s, \qquad 4.8$$

where $$T_o = 0.2 \cdot \frac{S_{D1}}{S_{DS}} \qquad 4.9$$

$$T_s = \frac{S_{D1}}{S_{DS}}. \qquad 4.10$$

An example of a design spectra using the above procedure is shown in figure 4.2. However, this analysis will be using the maximum credible earthquake spectral response acceleration values for creating a design spectrum. The maximum credible earthquake spectrum exceeds the design spectrum by a factor of 1.5.

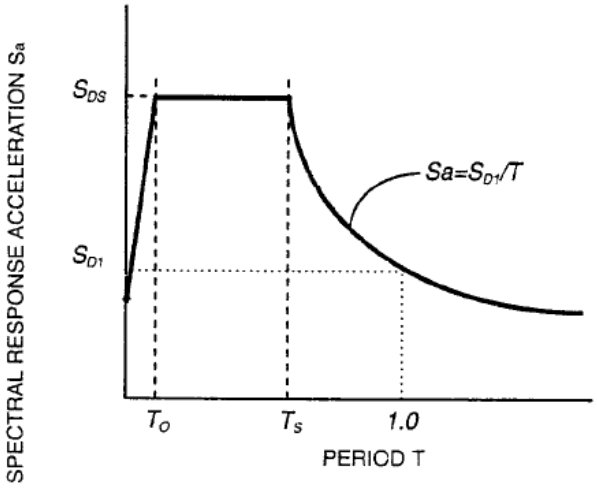

Figure 4.2: Example IBC design spectra. 2000 International Building Code. Copyright 2000. Falls Church, Virginia: International Code Council, Inc. Reproduced with permission. All rights reserved.

Chapter 5: Process and Analysis

Near-surface Models

This analysis uses results derived from a geotechnical engineering method called Cone Penetration Testing, or CPT, to attain information about the near-surface materials. This method uses a modified drill rig that pushes a sensor down to a desired depth. See figures 5.1a and 5.1b for a schematic showing the CPT method. The sensor tip is a cone of known area and will be used to measure cone tip resistance and friction behind the cone tip (sleeve friction). These basic measurements are used to characterize layers of different materials. A CPT profile can be interpreted as a geologic profile, based on correlations of material properties with the measured test parameters such as cone tip resistance, sleeve friction, and pore pressure. The cone tip resistance, sleeve friction, and pore pressure are sampled frequently and yield a continuous vertical profile, whereas other forms of geotechnical testing sample discontinuously. Also, CPT results are highly repeatable, as compared to other sub-surface testing methods (e.g. hollow-stem auger, Standard Penetration Testing).

Note that the CPT method does not return samples of the soil and stiff materials can prevent the cone from proceeding to greater depths. Because the soil is not directly sampled, soil type must be indirectly inferred and in some cases, the soil type remains ambiguous.

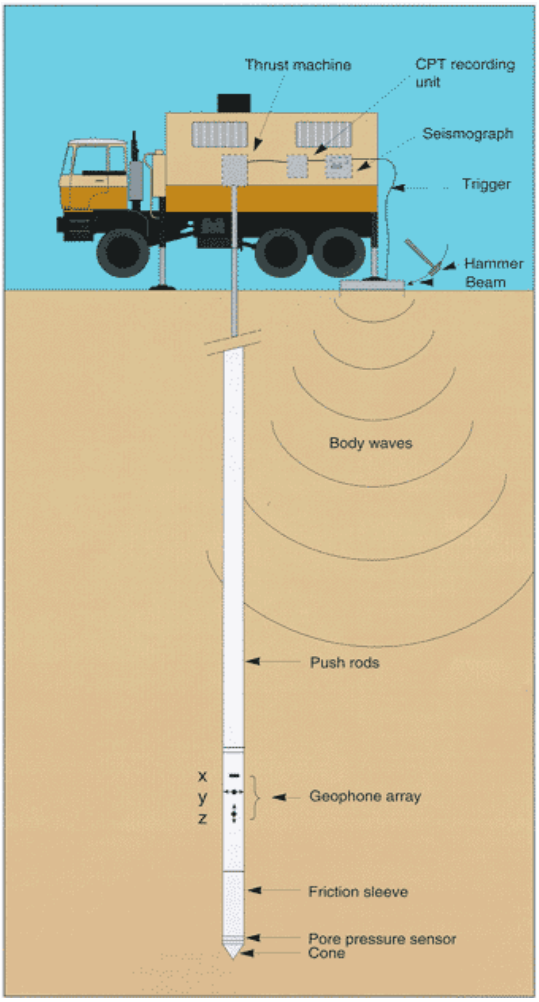

Figure 5.1a: Overview of Seismic Cone Penetration Testing method . Courtesy of Fugro Geosciences, Inc., used with permission.

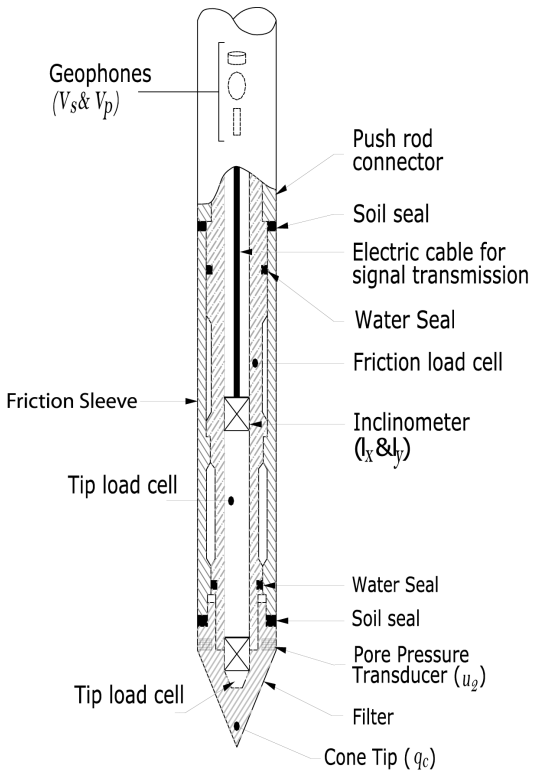

Figure 5.1b: Schematic of the sensor used in Cone Penetration Testing. Courtesy of Gregg Drilling, Inc., used with permission.

One of the advantages of CPT is that different sensors, including geophones, can be used to record seismic waves. The seismic CPT method uses a seismic source at the surface providing shear waves that are recorded in the subsurface by a geophone above the cone sensor. Shear waves are recorded at approximately 1.5 meter intervals. These data are used to determine shear wave interval velocities as a function of depth. An example of the data attained from a CPT sounding performed in the Charleston, South Carolina area is shown in figure 5.2.

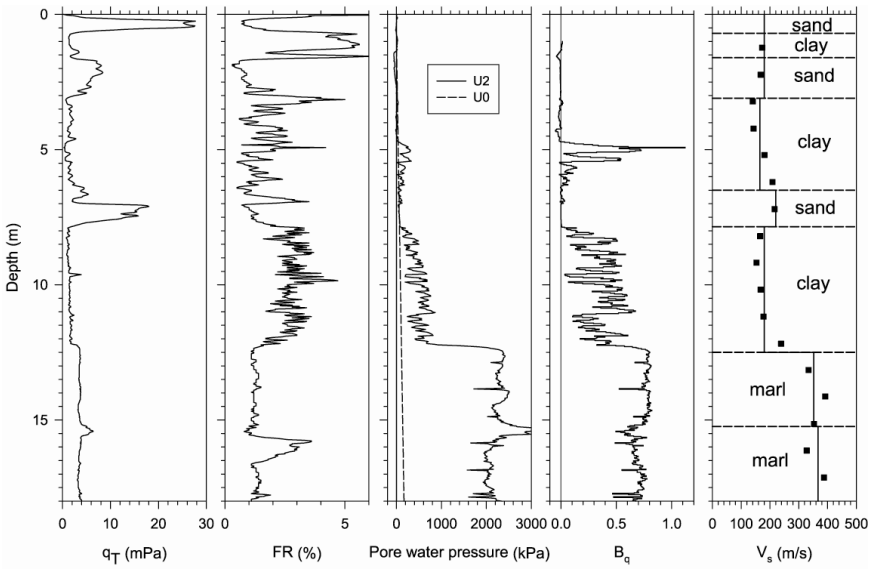

Figure 5.2: Example of cone penetration testing results, with the far right column being a shear wave velocity depth profile (Data provided by WPC Engineering, Inc., Mount Pleasant, SC).

Study Area

The selected study area is Columbia, South Carolina. This site is in an unusual situation because of its proximity to the Fall Line. Figure 5.3 shows the location of Columbia, South Carolina, on a general geologic map of South Carolina (Maybin and Nystrom, 1997). The black line in Figure 5.3 is an approximate location of the Fall Line which separates the Piedmont physiographic province from the Coastal Plain province and divides the Columbia region into two distinct near-surface environments.

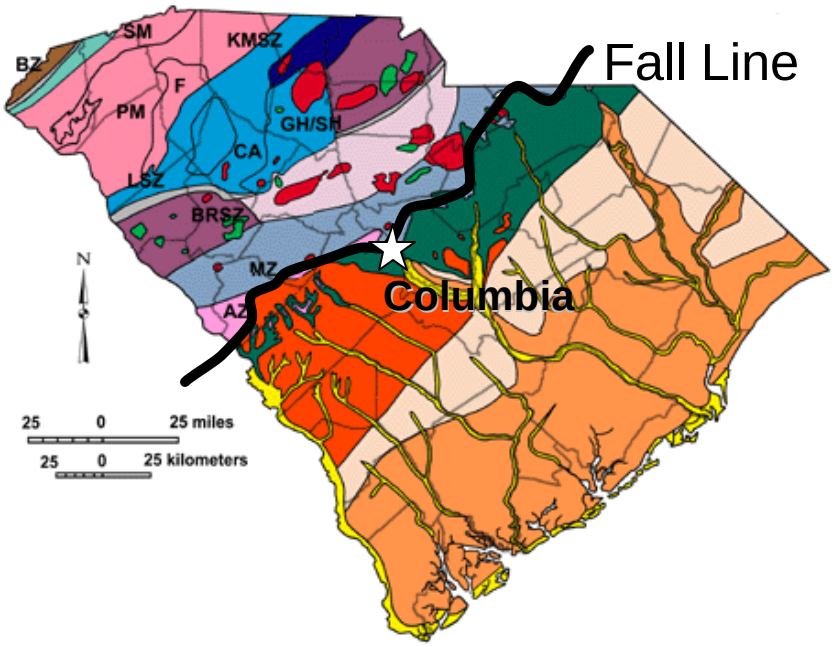

Figure 5.3: General Geologic Map of South Carolina. Columbia, South Carolina is shown by the white star and the thick black line is the approximate location of the Fall Line. (Generalized Geologic Map of South Carolina modified from Maybin and Nystrom (1997, South Carolina Department of Natural Resources, used with permission)

The northwestern portion of the city of Columbia lies on the crystalline bedrock that forms part of the Carolina Slate belt within the Piedmont. The slate belt in this area consists of metasediments and metavolcanic crystalline rock.

Columbia's southeastern portion is in the Coastal Plain province. The Coastal Plain consists of marine and fluvial sediments that thicken toward the coast. The thickness of the sediments is negligible at the Fall Line and increases to more that 1000 meters at the coast in southern South Carolina. Downtown Columbia lies southeast of the Fall Line and the general near-surface structure involves a thin layer of sediments overlying crystalline rock.

The site condition for Columbia is different from that assumed in constructing the National Seismic Hazard Maps (Frankel et al., 1996, 2002). These differences are the subject of this chapter.

The analysis included data from four sites in the vicinity of Columbia, provided courtesy of the Gage Group, Inc. All of the sites are southeast of the Fall Line, where crystalline bedrock is overlain by a thin layer of sediments. Approximate locations of the four sites are shown in figure 5.4.

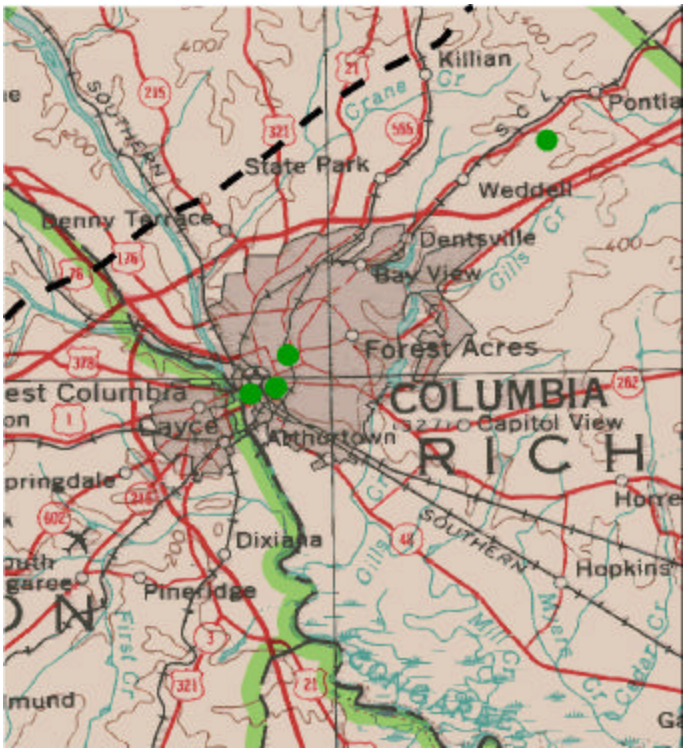

Figure 5.4: Approximate locations of geotechnical data in Columbia, SC (shown in green). The black dashed line is the estimated location of the Fall Line.

CPT data for Columbia, SC:

Figure 5.5 shows the shear wave velocity profiles for the four sites near Columbia. The depths sampled range from 13 meters to 33 meters and shear wave velocities range from 175 to 580 meters per second. The shear wave velocity information from the seismic CPT investigations is in the form of interval velocities determined at intervals Δz of approximately 1.5 m. Travel time t_i is measured at depth $i\,\Delta z$ where $i = 1,2,\ldots.n$. An interval velocity v_i is

calculated from $v_i = \Delta z / (t_i - t_{i-1})$. Given strong signal sources at the surface, the interval velocities can be determined with negligible error. However, the real Earth is not necessarily horizontally layered, and the velocity discontinuities in the sub-surface do not coincide with the depths at which interval velocities are measured. Clearly, velocity variations occurring over depth intervals smaller than Δz are not resolved, and the investigation produces a "smoothed" version of the sub-surface velocity profile. We interpret the interval velocities v_i to exist in n layers, each of thickness Δz, with the mid-depth of each later at $\Delta z(i - ½)$ meters below the surface. This is an approximation of the actual sub-surface condition.

The CPT soundings cannot be extended into the crystalline bedrock and the subsurface properties immediately below the depth of maximum penetration are unknown. Crystalline rock of the Carolina Slate Belt with very high seismic wave velocity is known to exist at depth; however, the velocity versus depth function, in the transition depth range from the base of the CPT profile to the basement rock at depth, is not known. This zone of transition involves partially weathered rock and residual soils that are so stiff as to stop cone penetration well before the intact crystalline basement is encountered. This material presumably has shear wave velocities intermediate in value between that of the softer sediments penetrated and that of unweathered crystalline basement.

The V_s or average soil shear wave velocity for the upper 30 meters and the site classification, as discussed in chapter 4, for each site are also shown in figure 5.5. Sites 1, 3 and 4 classified as D sites. Site 2 classified as C and will have a lower spectrum relative to the other sites, according to IBC 2000 procedures. This topic will be discussed further in the results section. The soil profile from soil borings and the velocity profile for each site are shown in

figure 5.5a through 5.5d. The materials encountered were sands, sand and gravel, clay, and partially weathered rock according to the soil boring logs provided by The Gage Group, Inc.

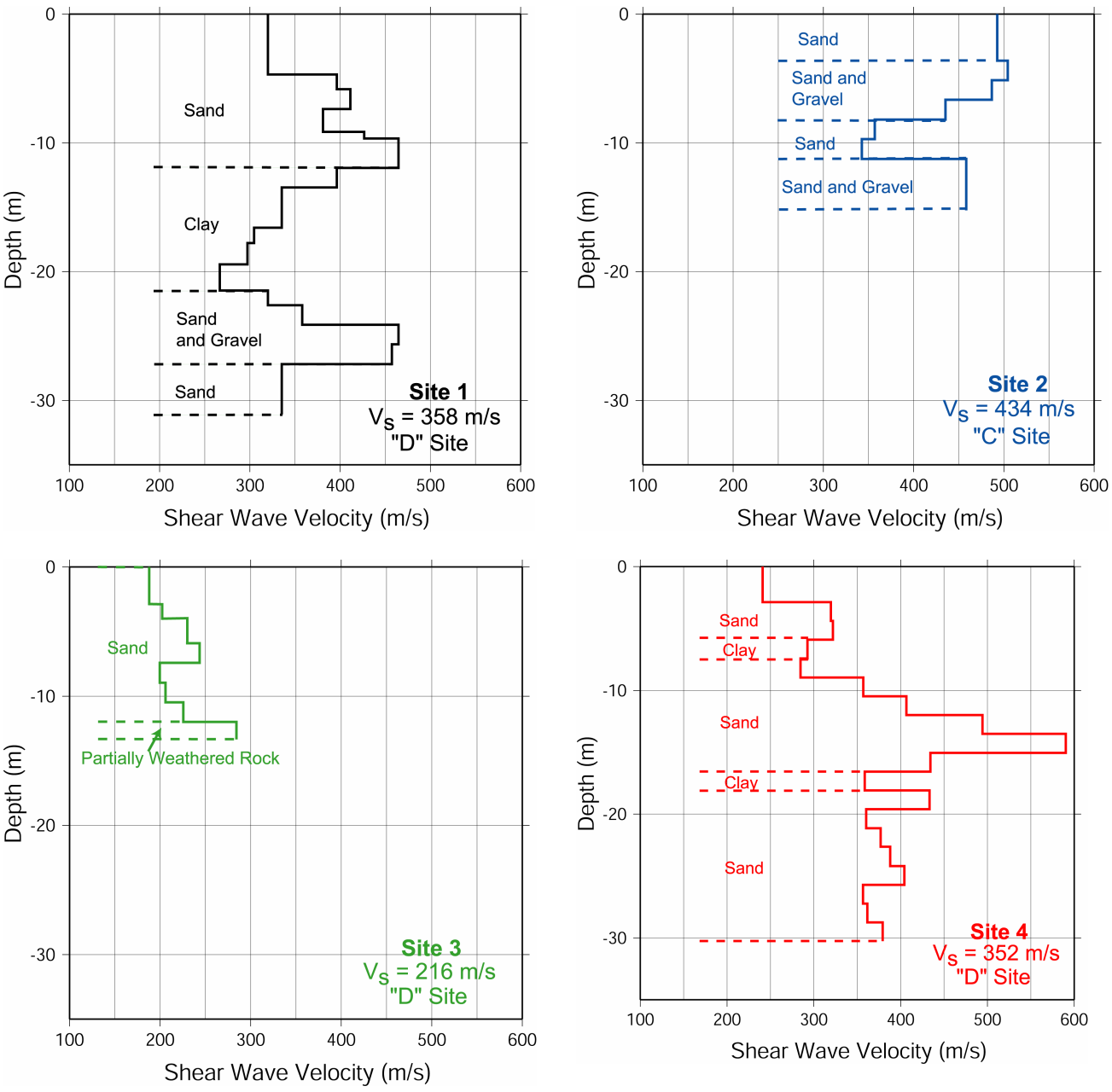

Figure 5.5: Soil profiles and shear wave velocity profiles for each site in Columbia. The soil boring data is provided courtesy of The Gage Group, Inc. The average soil shear wave velocity for the upper 30 meters and the IBC 2000 site classification for each site are also provided.

Different near-surface models

Various assumptions concerning the nature of the velocity transition between the CPT profile and the crystalline basement are investigated below. Various models of this transition are tested by calculating the response on the ground surface at the four sites, using scenario earthquake input motions consistent with the National Seismic Hazard Maps and IBC 2000. A goal of the study is to compare the site response determined by assuming a basement-soil transition zone with the direct imposition of B-C site conditions at the base of the CPT sampled profile. The latter approach is implied by the IBC (2000) building code and is commonly used by engineering firms in the study region. Our investigations will determine whether or not significant differences in the modeling approaches exist and, if so, under what conditions can the IBC procedures result in non-conservative spectra for design purposes.

Recall that the National Seismic Hazard Maps are prepared for B-C boundary site conditions, where B-C refers to an average shear wave velocity of 760 m/s for the upper 30 meters. This shear wave velocity value exceeds that of all materials sampled by the seismic CPT at the four sites examined in Columbia, S.C. As discussed above, crystalline rock is known to exist at shallow depths at these sites. The seismic CPT is terminated when the cone reaches the partially weathered crystalline rock material that prevents further penetration. The thickness of this weathered rock zone is not known from direct measurement; although, a range of reasonable thickness values at the four sites can be inferred from previous experience of the local engineering community (Phillip Morrison, personal communication, 2004). Velocities of 760 m/s are reached at unknown depth in this weathered zone and presumably increase with depth in some fashion until unweathered basement rock is reached. Therefore, two different models are developed to estimate the effects of the unknown subsurface properties for the purpose of

comparison: 1) application of input motion consistent with B-C outcrop conditions directly at the bottom of the profile sampled by the geotechnical data and 2) application of the input motion consistent with bedrock outcrop conditions at the base of a weathering transition zone consisting of a velocity gradient. The velocity gradient is modeled with 16 discrete layers. The thickness of the layers is treated as a random variable and will be discussed in more detail below. This transition zone immediately underlies the materials sampled by geotechnical investigation. Figure 5.6 shows the two near-surface models with the model for B-C outcrop conditions model shown in green and the model for rock outcrop conditions model shown in blue.

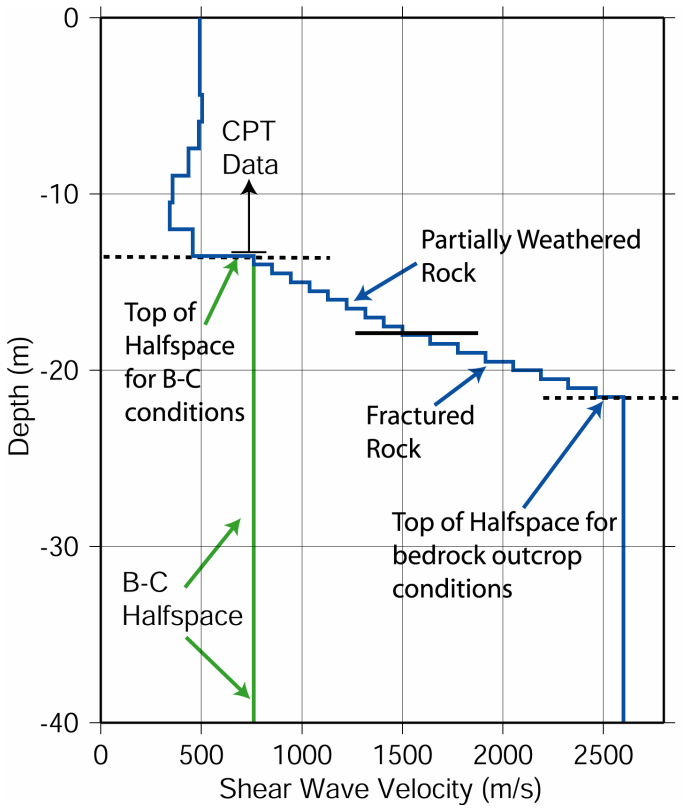

Figure 5.6: Different subsurface models for site 2. The B-C outcrop model is shown in green and the rock outcrop model is shown in blue. Similar models were constructed for sites 1, 3 and 4. The models differ only in the shallow depth range sampled by seismic CPT data.

The model using B-C outcrop input motion assumes that a halfspace consisting of a shear wave velocity value of 760 meters per second underlies the seismic CPT velocity profiles at each site. The B-C outcrop conditions are the same conditions represented in the National Seismic Hazard Maps and used in IBC 2000.

The shear wave velocity gradient in the rock outcrop input model represents the transition zone of weathered and fractured rock overlying crystalline bedrock. Our estimate of the weathered rock and underlying hard rock velocities are based on measurements made near Lake Murray, South Carolina by Odum et al. (2003) and measurements in southeastern Canada by Bersnev et al. (2002). Lake Murray is located approximately 20 kilometers to the northwest of downtown Columbia. Odum et al. report a shear wave velocity of 1184 m/s in the shallow weathered zone of the Carolina Slate Belt in the depth range of 5 to 25 meters. At depths exceeding 25 meters, Odum et al. find shear wave velocities of 2674 m/s, in Slate Belt rock. The value of 2674 m/s is representative of shear wave velocity measurements reported by Beresnev et al. (2002) for hard rock exposures in southeastern Canada. On the basis of this, a shear wave velocity of 760 m/s is adopted (B-C boundary or firm rock) for the top of the transition zone and 2600 m/s for the base of the transition zone. Experience from rock core sampling and strength measurements at hard rock sites in the Columbia area (Phillip Morrison, personal communication, 2004) provides some range of estimates for likely thickness of the weathered and fractured rock zone at the four sites.

Input Motions

The process for calculating synthetic time series that is used as the input motion for the site response analysis is outlined in Chapter 3.

Deaggregation

The seismic hazard results for 2% probability of exceedance in 50 years of exposure for the downtown center of Columbia (33.993°N, -81.005°W) determined by Frankel et al. (2002) are assumed to apply to all four sites. Deaggregation matrices for oscillator frequencies of 0.5, 1.0, 2.0, 3.33, 5.0 and 10.0 Hz, as well as peak ground acceleration (PGA) indicate that the dominant scenario event should correspond to a magnitude 7.3 earthquake at an epicentral distance of 123 km. Figure 5.7 shows the Frankel et al. (2002) deaggregation for peak ground acceleration in Columbia.

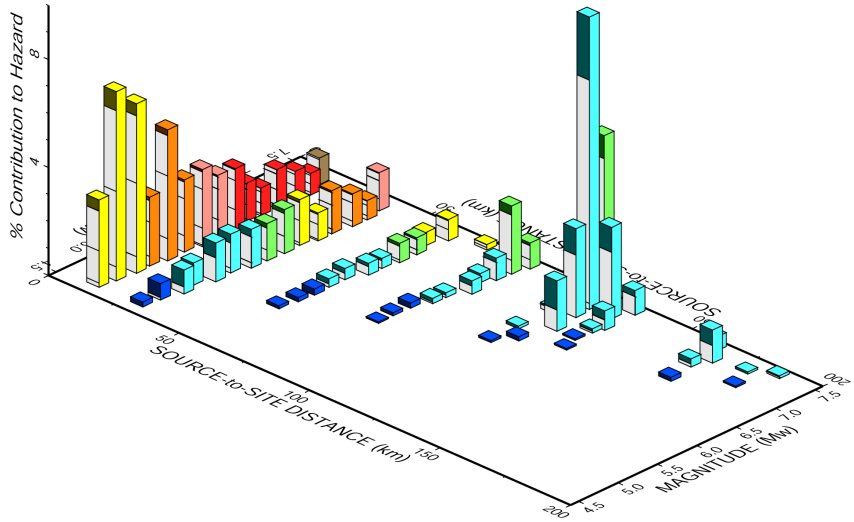

Figure 5.7: Peak ground acceleration deaggregation for Columbia, SC from USGS National Seismic Hazard Mapping Project website: http://eqint.cr.usgs.gov/eq/html/deaggint2002.html

The deaggregation is essentially independent of the assumed B-C boundary site condition and the Frankel et al. (2002) deaggregations can be used for hard rock sites as well. With the scenario earthquake defined, the stochastic method described in Chapter 3 is used to simulate appropriate ground motions for hard basement rock outcrop conditions. This motion is shown in part A of figure 5.8.

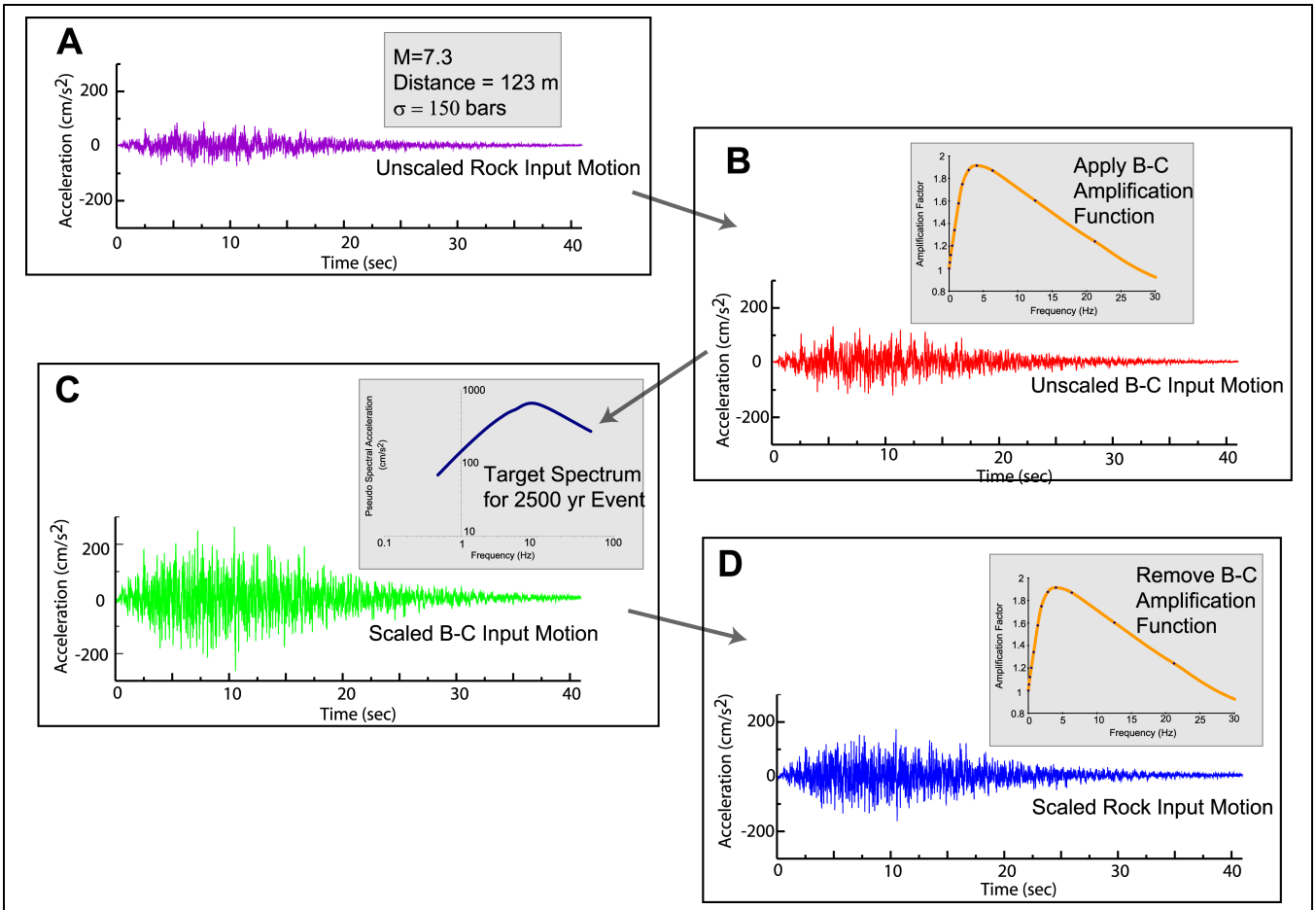

Figure 5.8: General process for developing input motion. The scaled B-C time series and the scaled rock time series are the input for the equivalent linear analysis.

IBC 2000 and the National Seismic Hazard Maps are calibrated to B-C boundary site conditions. Therefore the time series must be adjusted to match the conditions assumed for the National Seismic Hazard Maps and IBC. Recall from Chapter 4 that B-C conditions are considered "firm-rock" conditions and correspond to an average shear wave velocity of 760 meters per second. The amplification function used in the National Seismic Hazard Maps for the B-C conditions shown in figure 5.9. This function is defined in appendix A of Frankel et al. (1996) and is based on the amplitude response of a generic soil profile, assuming anelastic attenuation defined by kappa equal to 0.01. The time series with the B-C site conditions amplitude response applied is shown in part B of figure 5.8.

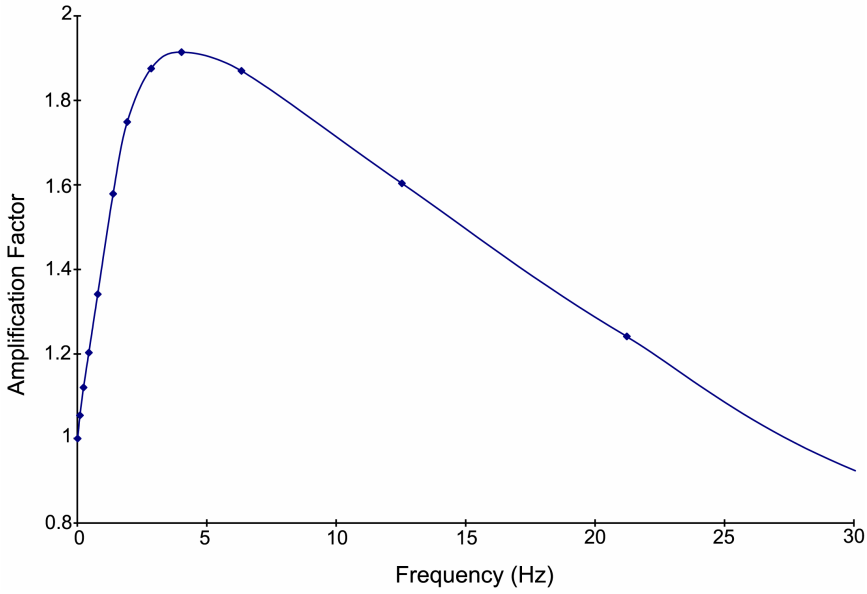

Figure 5.9: Amplification for B-C outcropping conditions from Appendix A in Frankel et al. 1996.

Because the scenario earthquake (M=7.3, at a distance of 123 km) dominates the seismic hazard at Columbia, the shape of the 2475 year return period (2% probability of exceedance in 50 years) uniform hazard spectrum is very similar to that of the scenario earthquake. In this case, representing the uniform hazard spectrum with a single scenario event is appropriate. The uniform hazard spectrum for Columbia is shown in figure 5.10 for the 2475 return period from Frankel (2002).

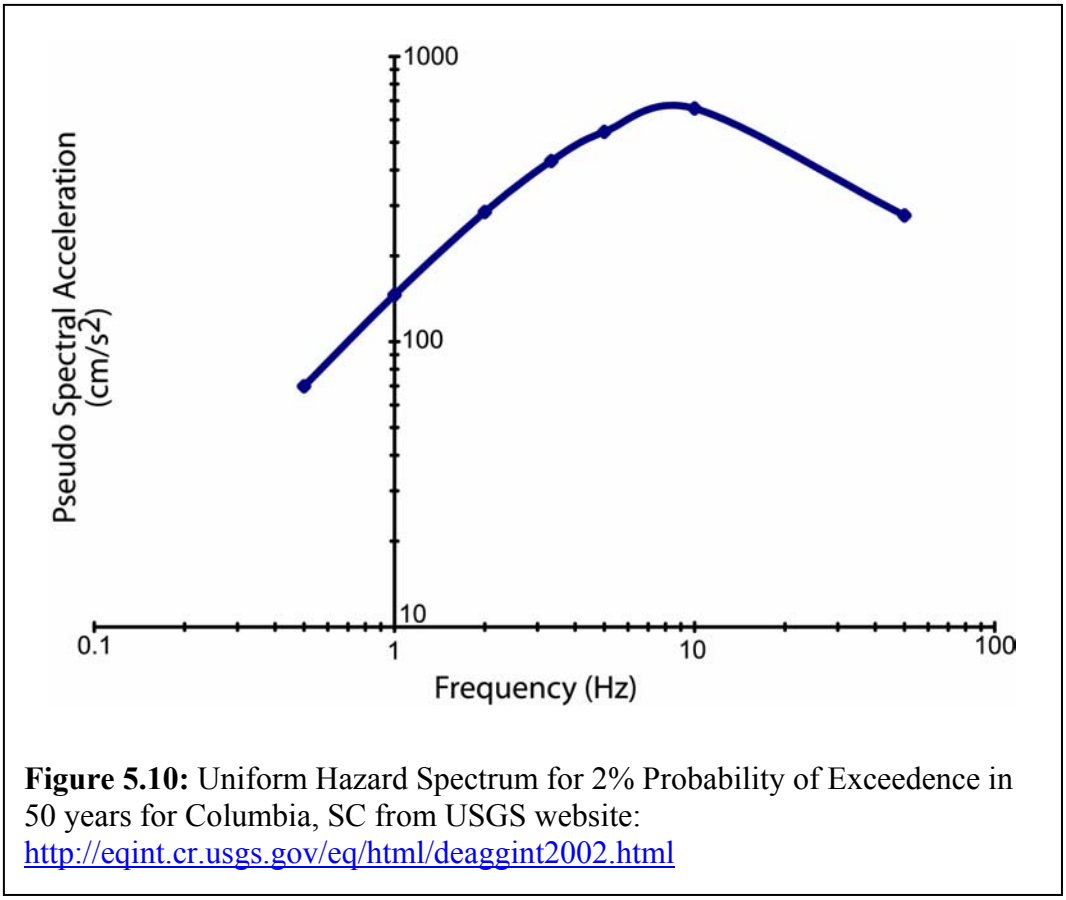

Figure 5.10: Uniform Hazard Spectrum for 2% Probability of Exceedence in 50 years for Columbia, SC from USGS website: http://eqint.cr.usgs.gov/eq/html/deaggint2002.html

The mean return period of the scenario shock (M = 7.3 in the Charleston source area) is approximately 500-1000 years as modeled in the National Seismic Hazard Maps. Because the hazard level selected by IBC 2000 represents a mean return period of 2475 years, the uniform hazard spectrum exceeds the amplitude of the median motions of the scenario event. To match the uniform hazard spectrum, it is necessary to scale the synthetic input motions developed on the basis of the M = 7.3 at a distance of 123 kilometers.

The result of scaling of the synthetic input time series for the B-C outcrop conditions to match the uniform hazard spectrum for Columbia is shown in part C of figure 5.8. This scaling is done using a phase-invariant, iterative approach. This approach involves the following steps:

1) The Fourier amplitude spectrum of the scenario earthquake acceleration time series on B-C outcrop is calculated.

2) The PSA response spectrum of the scenario earthquake is calculated and interpolated using a cubic spline fit for the Fourier frequencies defined in step 1 above.

3) The 2475 year return period PSA uniform hazard spectrum defined by Frankel et al. (2002) is interpolated at the same Fourier frequencies and serves as a "target" spectrum.

4) The ratio of the interpolated target to scenario PSA spectra is calculated at the Fourier frequencies.

5) The Fourier amplitude spectrum of the scenario event is multiplied by the ratio defined in step 4 above. The Fourier phase spectrum is not altered.

6) The result of step 5 is transformed to the time domain.

7) Steps 1 through 6 are repeated as necessary until visual satisfactory agreement between the PSA motion of the time series and the target PSA spectrum is reached.

The second set of input models examined the application of hazard consistent input motions at the base of a linear velocity gradient. This suite of models, for the four sites, is referred to as “rock outcrop” and is shown schematically in the right portion of figure 5.15. The input motion for the rock outcrop condition is derived from the scaled B-C outcrop motions shown part C in figure 5.8 by first removing the B-C amplitude response as shown in part D of figure 5.8 (frequency domain division). A second modification is made by increasing the amplitude of the input motion by a factor of 1.2 to account for the velocity decrease from that at seismogenic depth (assumed to be 3500 m/s) to that at the base of the weathered zone in the shallow crust (here assessed to be 2600 m/s).

The amplification factor of 1.2 applied to the input motion is based on the following equation from Shearer and Orcutt (1987). This equation is for total transmission in materials where velocity and density vary smoothly:

$$\frac{A_2}{A_1} = \left[\frac{\rho_1 V_1}{\rho_2 V_2} \right]^{1/2}, \qquad 5.1$$

where A_2 is the calculated seismic amplitude after passing through the material, A_1 is the initial amplitude of the seismic wave, ρ is the density of the material and V is the seismic velocity of the material. We assume that: ρ_1 and ρ_2 are equal to 2600 kg/m3, V_1 equals 3500 m/s (at earthquake focal depth) and V_2 equals 2600 m/s (at the base of the velocity transition zone). The result of this operation produces a ground acceleration input motion representing motion on hard rock outcrop with a 2% probability of exceedence in 50 years in figure 5.13.

Figure 5.11 shows the frequency spectrum of all the time series discussed and the target spectrum for the 2500 year event. Notice that the scaled B-C time series and the target spectrum match closely.

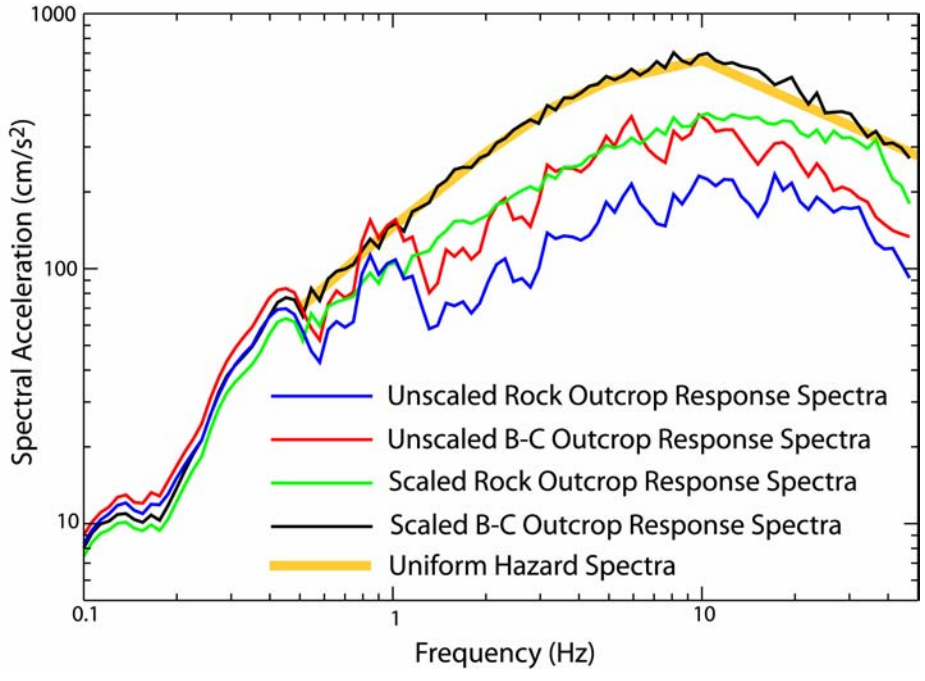

Figure 5.11: Response Spectra for the input time series and the uniform hazard spectrum.

Results

The surface motion is calculated using the equivalent linear algorithm from Schnabel, Lysmer and Seed (1972) as implemented in the program created by Dr. Martin Chapman (2004). (Chapter 2 discussed both topics in detail.) The B-C outcrop input motion and bedrock outcrop input motion were applied to each of the four sites. In the case of the rock input model, a velocity gradient was inserted above the bedrock and below the base of the CPT sampled velocity profiles. See figure 5.12 for a schematic of the two input models.

The initial analysis used an 8 meter thick velocity gradient in the rock outcrop model with a shear wave velocity of 760 meters per second at the top increasing stepwise to 2600 meters per second at the bottom in 0.5 meter thick layers. Figure 5.12 shows both the models for bedrock outcrop input and B-C outcrop input and the respective input and surface time series.

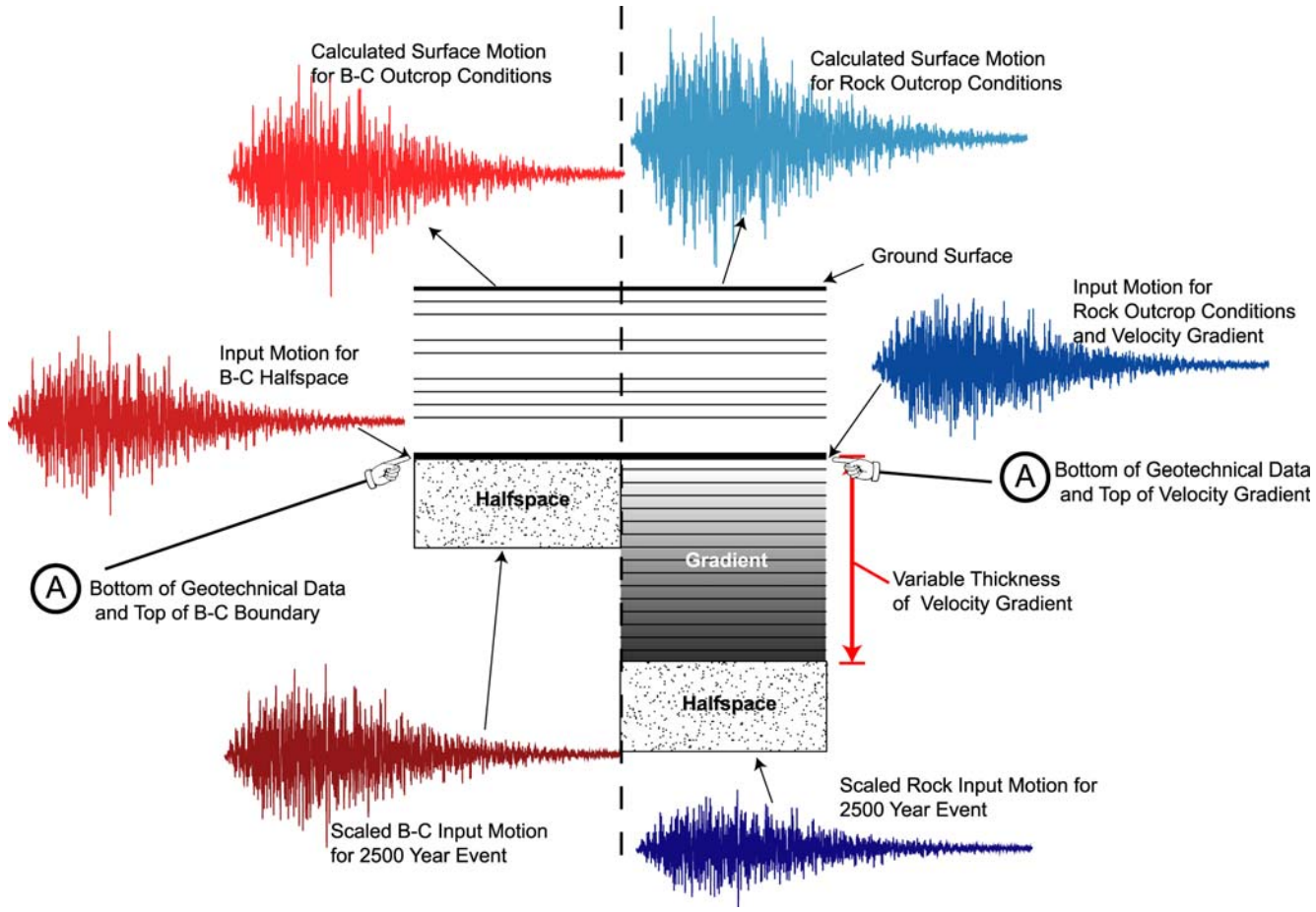

Figure 5.12: Comparison of B-C and rock outcropping models. The dashed line separates the two models with the B-C outcropping model on the left and the bedrock outcropping model on the right. Notice point A that is the interface of the bottom of the geotechnical data and the top of the B-C halfspace and the velocity gradient.

The spectral acceleration of the calculated surface motion for each site are shown in figure 5.13, for the B-C outcropping model conditions, and figure 5.14, for the bedrock outcropping conditions. The response spectra for the B-C conditions will be used for comparison with the IBC 2000 maximum credible earthquake (MCE) spectra in the following paragraphs. Figure 5.14 shows only a single scenario of the subsurface for the rock outcropping conditions model, which may or may not represent the actual conditions present at the site. Because of the uncertainty of the partially weathered and fractured rock region, the rock

conditions response spectra will be further analyzed by modeling different thicknesses of the velocity gradient to produce a range of response spectra.

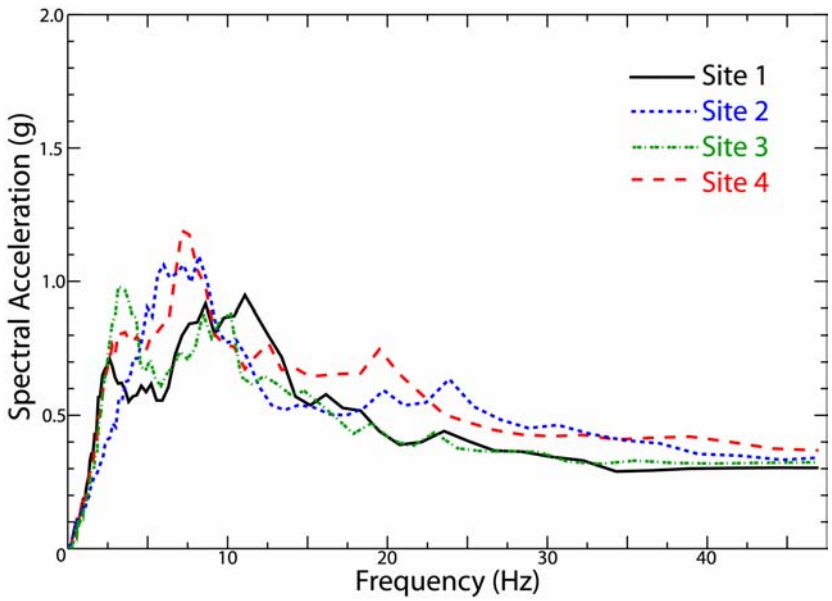

Figure 5.13: Response Spectra for calculated surface motion using the scaled B-C input motion.

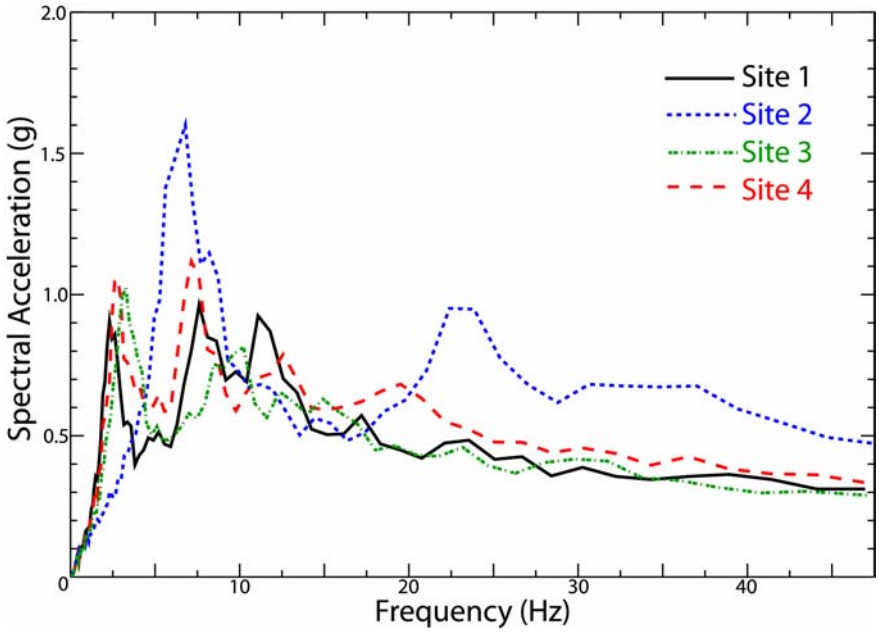

Figure 5.14: Response Spectra for the calculated surface motions using the scaled rock input motion, with 8 meter thick velocity gradient.

Various material properties and behavior of each site derived from the equivalent linear algorithm analysis, for the B-C conditions model and rock conditions model with 8 meter thick velocity gradient, are shown in figure 5.15. The graphs, from left to right, are: shear wave velocity, effective shear strain, normalized shear modulus and damping ratio. All of the parameters are plotted as a function of depth and are at the same scale for the individual sites. The low velocity layers exhibit maximum shear strains, minimum values of normalized shear modulus (G/G_{max}), and maximum values of damping. For example, site 1 has a low shear wave velocity extreme at 20 meters depth, which results in strains on the order of $5x10^{-4}$, normalized shear modulus of 0.6, and damping of 7% critical. The remaining three sites have similar correlations for low velocity regions.

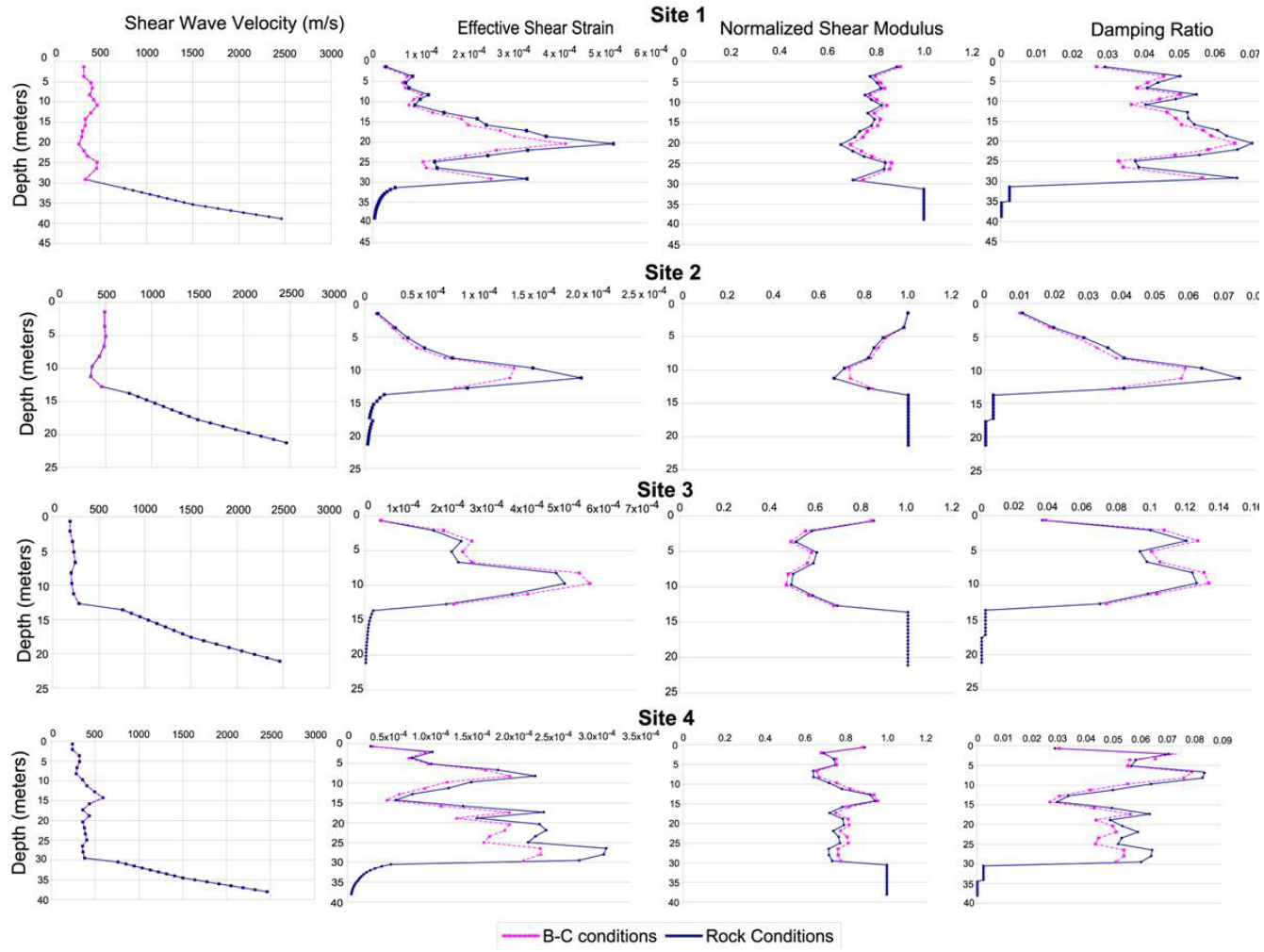

Figure 5.15: Material properties versus depth for each site. The graphs show, from left to right: shear wave velocity, effective shear strain, normalized shear modulus and damping ratio. The B-C conditions response is the dashed line while the solid line is for the rock conditions model with an 8 meter thick velocity gradient.

Randomization

The rock conditions model is an attempt to define a geologically realistic scenario. The direct measurement of velocity as a function of depth is limited to the shallow subsurface investigated by the seismic CPT tests. The existence of a velocity transition zone is inferred between the base of the sampled profile and hard rock conditions at depth. Because the thickness of the transition zone is uncertain, it is treated as a random variable. The sensitivity of the calculated response to the uncertain thickness of this zone is examined by randomizing the

thickness of the velocity gradient. From discussions with experienced local engineers (Phillip Morrison, personal communication), the thickness of this zone is modeled as ranging 0 to 40 meters.

Figure 5.14 shows results for one possible scenario with the velocity gradient being 8 meters thick. Several analyses were made using different velocity gradients with variable thickness. The partially weathered rock and fractured rock zones were modeled separately as two distinct zones. The thickness of each zone was treated as a random variable with a uniform probability distribution over the range of 0 to 20 meters. Ninety-nine realizations of the random rock conditions model were computed using the equivalent linear algorithm. The distribution of the randomized total thickness for the velocity gradient zone is shown in figure 5.16. Selection of the two uniformly distributed thicknesses for the partially weathered rock and fractured rock zones, respectively, results in a general Gaussian shape for the distribution of the total thickness of the velocity gradient.

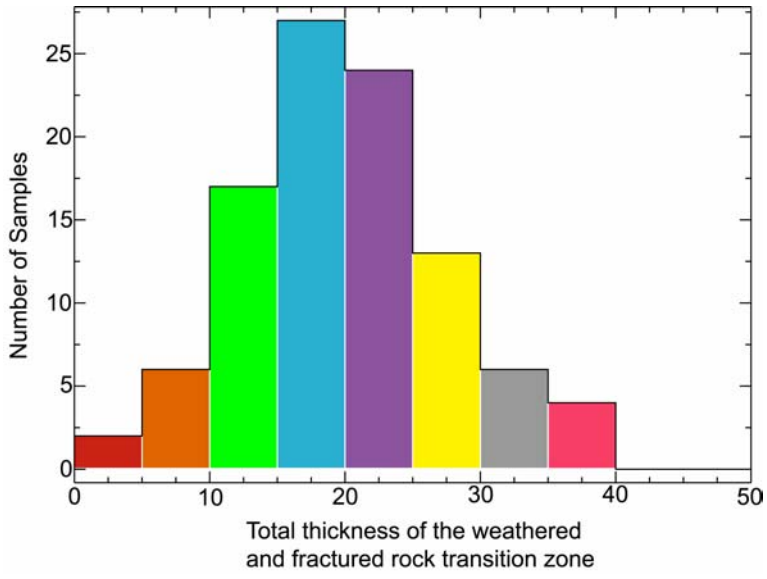

Figure 5.16: Distribution of the total thickness of the weathered rock and fractured rock zone used by the randomized model for the rock outcrop conditions.

Figure 5.17 shows the 0, 50, and 100 percentile spectral acceleration for the rock conditions model, at the top of the velocity gradient for outcrop condition (point A in figure 5.12). The figure also shows spectral acceleration for B-C outcrop conditions (also, point A in figure 5.12). The B-C spectral acceleration has a peak value of 0.7g between 7.5 to 10 Hz. The rock conditions model exceeds the B-C model for the majority of the simulations at frequencies greater than 10 Hz. This demonstrates that the effect of the transition zone, representing weathered and fractured rock, is to increase high frequency amplitude of the input motion at the base of the soft soil column.

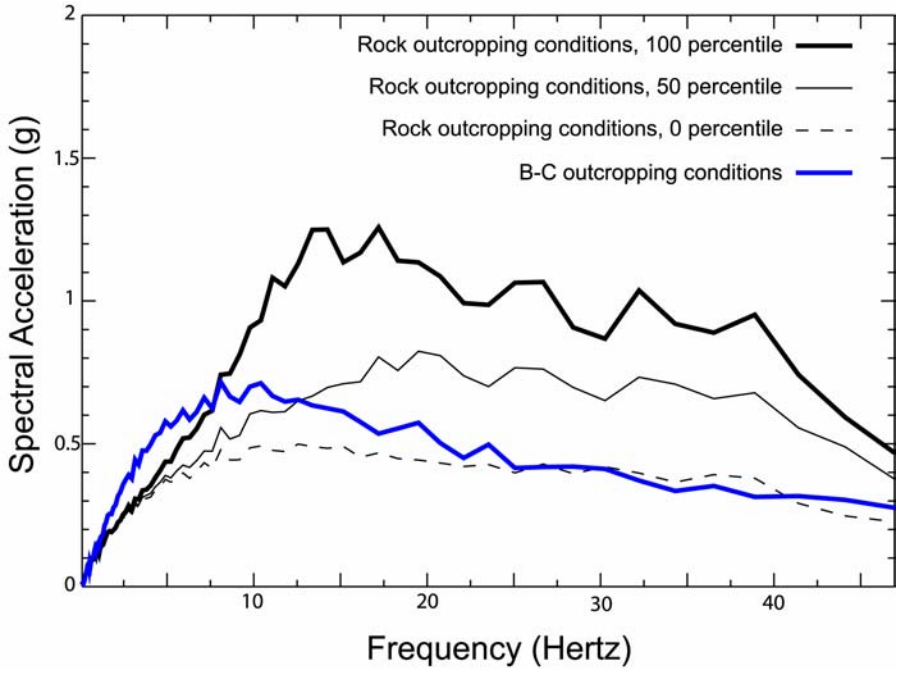

Figure 5.17: Spectral acceleration at point A in figure 5.15, the top of the B-C halfspace and the top of the velocity gradient.

Figure 5.18 shows the SA response on the ground surface for the four study sites using the rock condition model. Separate curves show the 0, 15, 85, and 100 percentile amplitudes of the 99 simulations.

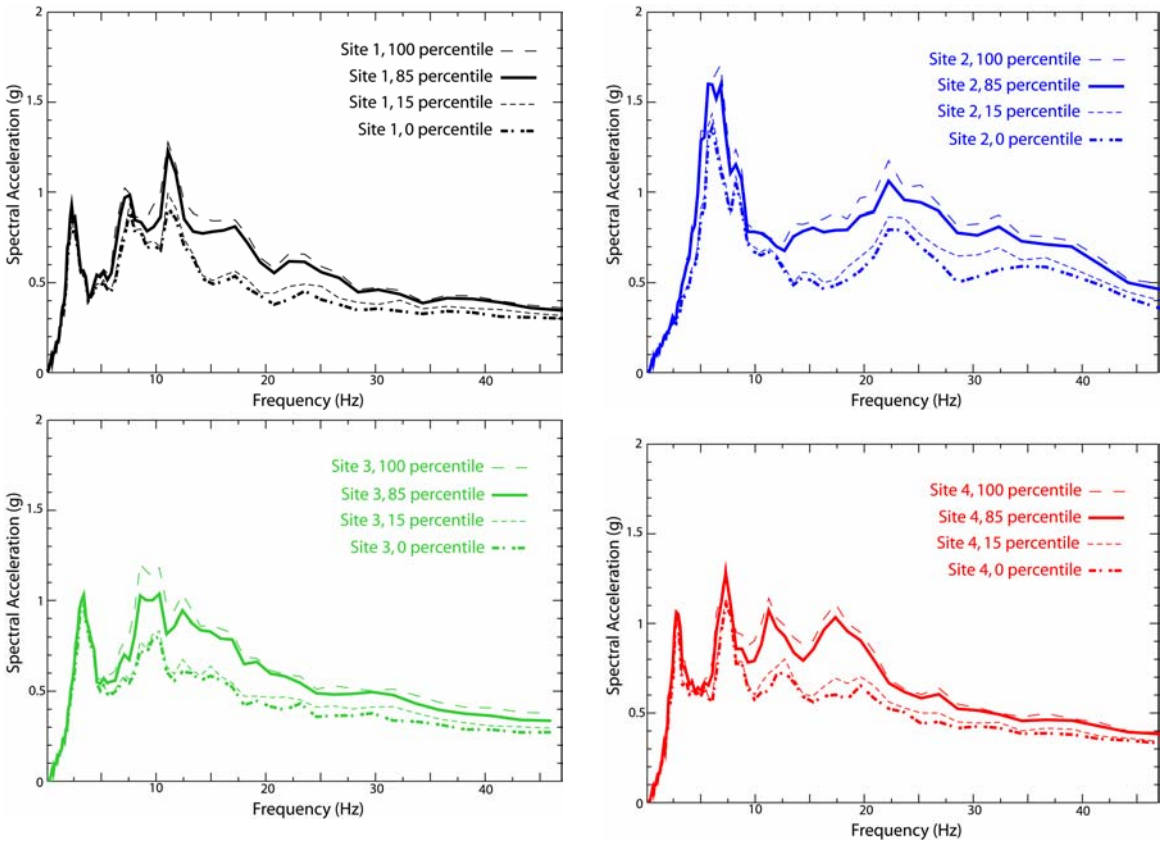

Figure 5.18: Spectral response percentiles for the randomized subsurface rock condition model for each site in Columbia. The 0, 15, 85, and 100 percentiles are shown.

Site amplification can be represented by the ratio of SA response from the ground surface to the SA response of "rock" material. Figure 5.19 shows the SA response ratio for B-C conditions and figure 5.20 shows the SA ratio for the model representing rock conditions.

Site 2 has the largest response by far of the four sites. The most outstanding feature of the response is the amplitude peak in the range 6 to 10 Hz. The other three sites have their fundamental resonance peaks at somewhat lower frequencies, in the range 2 to 5 Hz. The higher frequency peak response at site 2 is due to the fact that it has the highest average shear velocity of the 4 sites combined with a shallow depth to firm rock. This results in smaller vertical travel-time thru the sediments at site 2 compared to the other 3 sites. Also, there is a low velocity layer near the base of the sampled profile at site 2. This low velocity layer adjacent to the weathered

rock transition zone creates a substantial impedance contrast, with contributes to the large amplitude of the overall response.

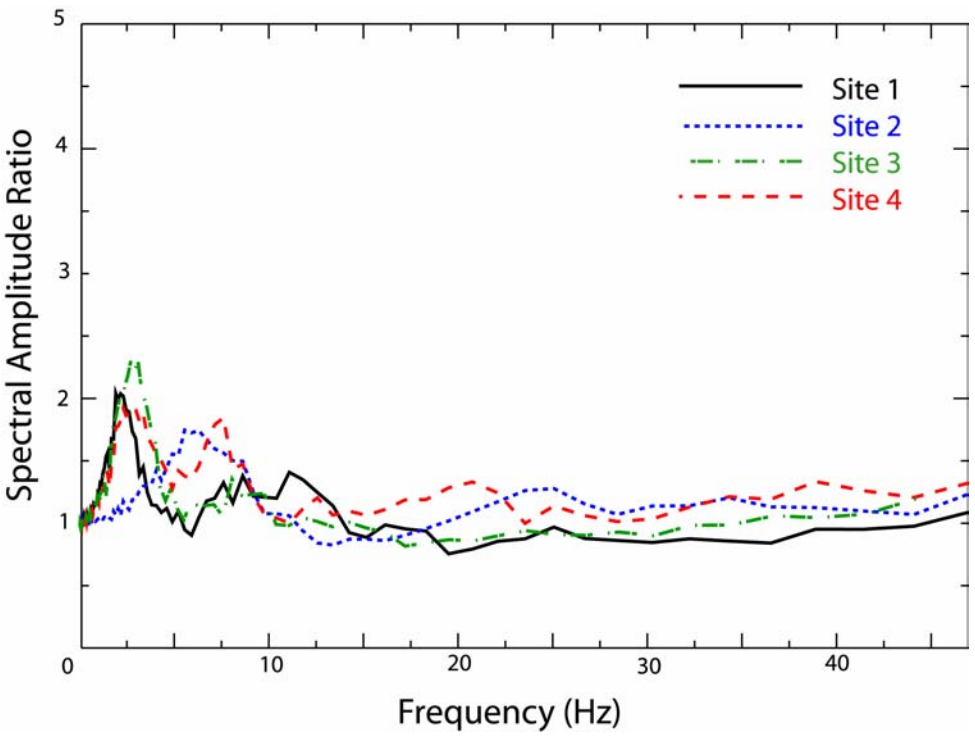

Figure 5.19: Spectral acceleration ratio for the four sites with B-C conditions.

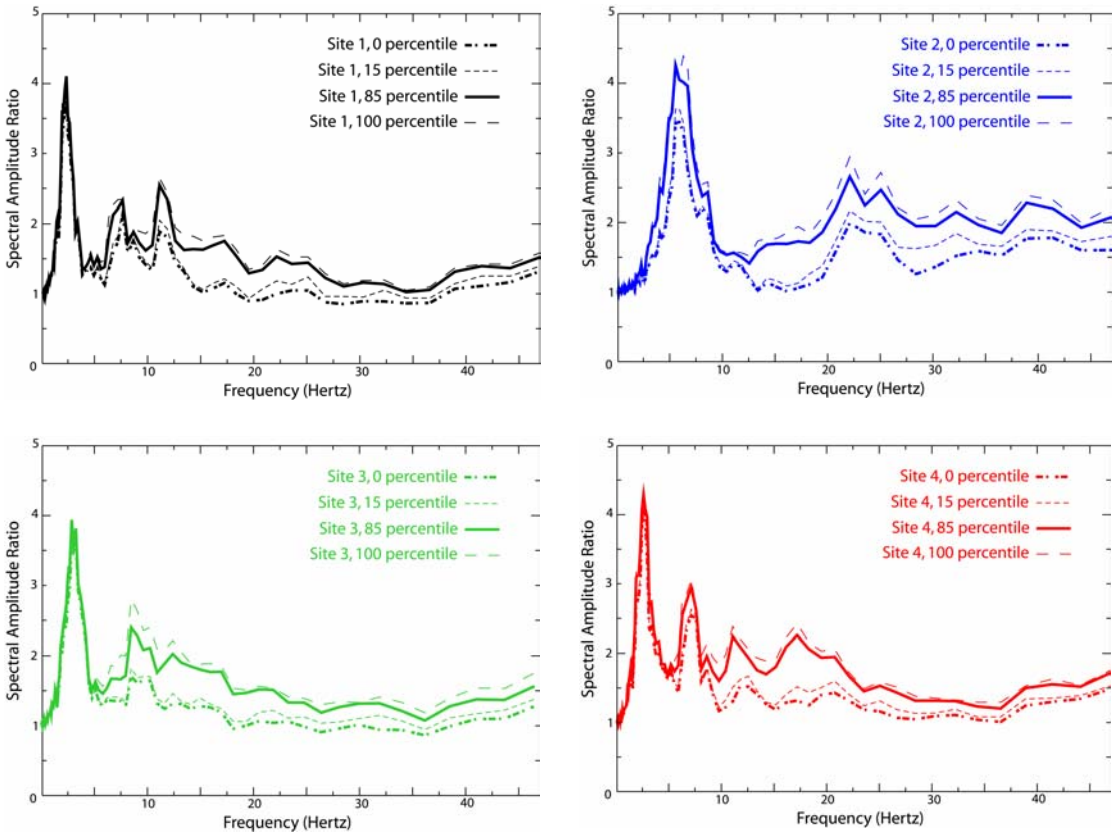

Figure 5.20: Spectral acceleration ratio with the randomized models for rock conditions. The 0, 15, 85, and 100 percentiles are shown for each site.

IBC spectra

Recall from chapter four, that the IBC 2000 response spectra are derived from the National Seismic Hazard Maps and subsurface geotechnical information. The average shear wave velocity in the top 30 meters or V_s is used to classify the site into a NEHRP category, shown in table 4.1. Three of the four sites for Columbia classified as D sites. The remaining site classified as a C site. Their respective IBC 2000 maximum credible earthquake response spectra are shown in figure 5.21. Note that the IBC 2000 maximum credible earthquake response spectra, IBC 2000 MCE response spectra, exceeds the IBC 2000 design response spectra by a factor of 1.5.

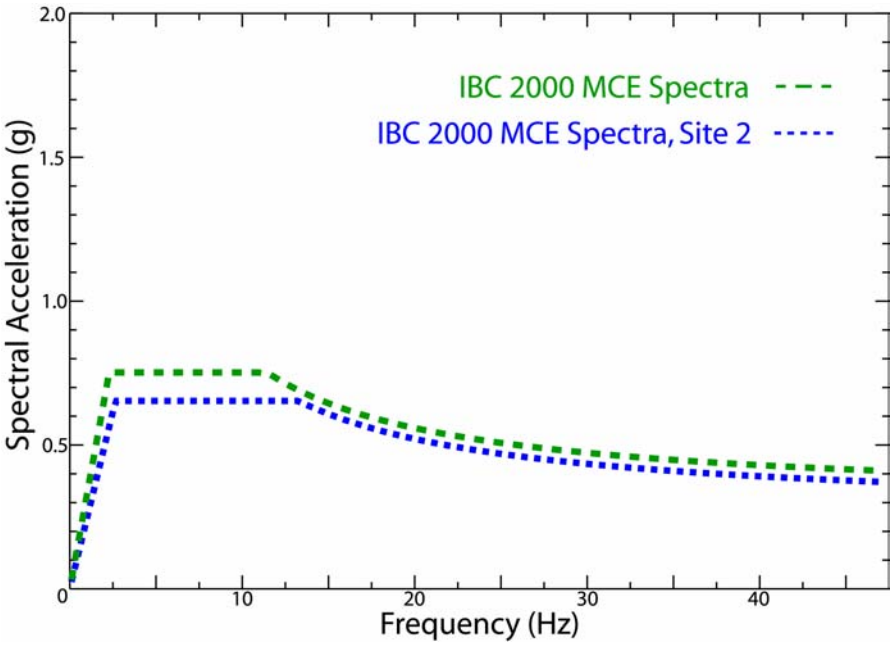

Figure 5.21: IBC 2000 Maximum Credible Earthquake response spectra for all four sites in Columbia, SC. Site 2 has a different curve because of its site classification.

Comparison of results to IBC 2000 MCE spectra

The IBC 2000 MCE response spectra are compared with the calculated response spectra for both B-C and rock outcropping conditions in figure 5.22. Both B-C and rock conditions response spectra exceed the IBC spectra at specific frequencies at all sites. For every site there are peaks, for both outcrop conditions, that lie above the flat portion of the IBC spectrum (2.5 to 11 Hz). Two features are prominent: large response peaks exceeding the IBC 2000 spectra occur at frequencies less than 10 Hz and are largest for the rock condition models. The second feature is an overall increase in the high frequency amplitudes (>5 Hz) in the case of the rock condition models. For example, the large response between 10 and 20 Hz for site 3 is due to the velocity gradient amplifying the signal for that frequency range, combined with resonance of the soil structure in that frequency band.

Site 2 has the largest response by far of the four sites and it is the most significant. Recall that this site was classified, using IBC 2000, as a C site. Because site 2 has a higher V_s, the IBC 2000 code considers it to be more competent material and prescribes a slightly lower spectrum than the other sites. The site 2 response spectrum markedly exceeds the IBC spectrum in the frequencies from 4 to 10 Hz. This applies for both B-C outcrop conditions and rock conditions, although most simulations using the rock conditions model considerably exceed the B-C outcrop model in this frequency band (figure 5.22). This frequency band is important because it corresponds to the band of structural response for single story construction. The other three sites feature fundamental site resonances at lower frequencies (2 to 3 Hz), with somewhat smaller amplitudes compared to site 2. The response of the rock outcrop condition model differs from the B-C outcrop model most prominently at frequencies greater than 7.5 Hz. Most of the randomly chosen simulations using the rock outcrop conditions substantially exceed the B-C outcrop conditions spectra at frequencies greater than 7.5 Hz (figure 5.22). The impedance of site 2 is greater in the rock input model than the B-C input model and is shown as having the greatest difference between the two input models response spectra. In summary, the geologically realistic model (rock outcrop conditions with a velocity gradient) exceeds the MCE spectrum prescribed by IBC 2000 code procedures.

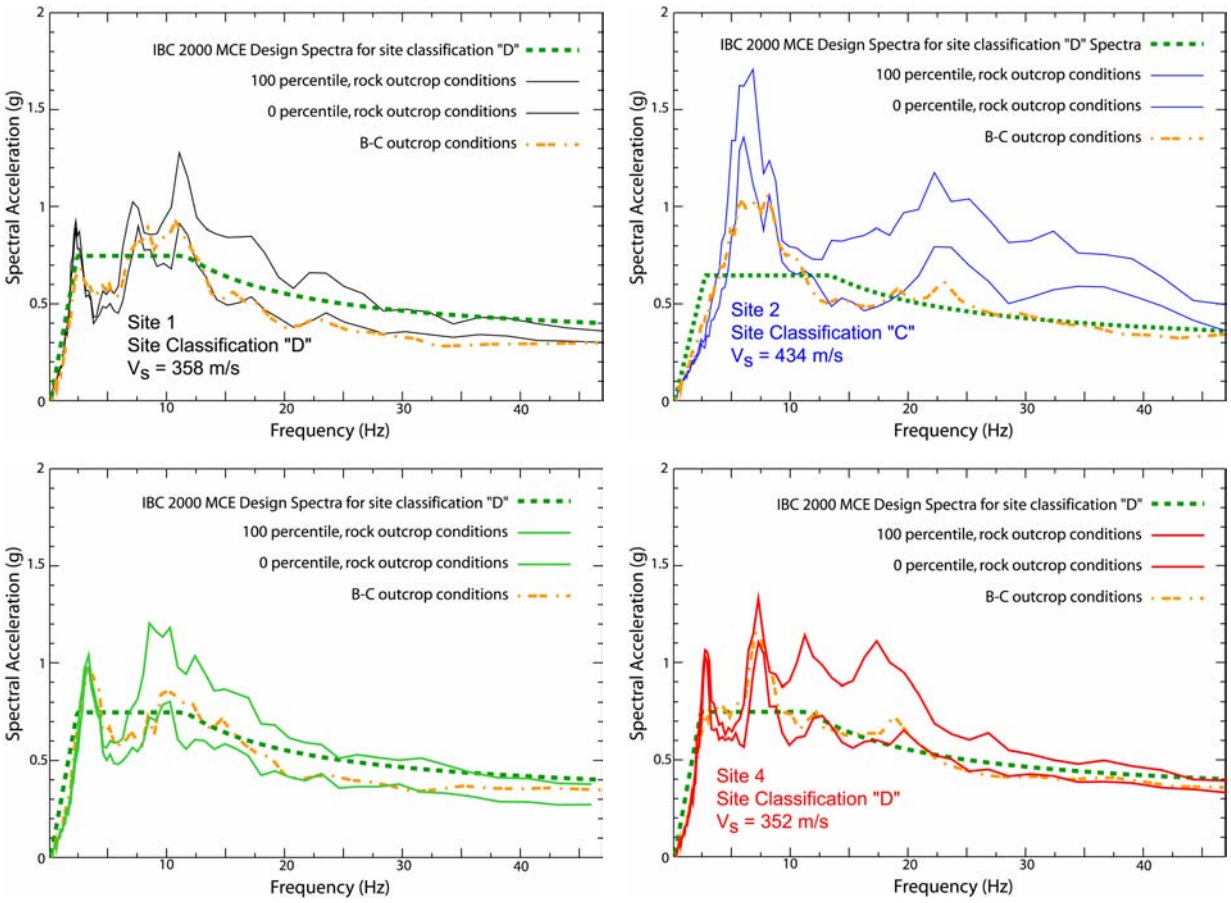

Figure 5.22: Spectral acceleration for each site with B-C conditions and rock conditions with the randomized velocity gradient thickness percentiles shown. The appropriate IBC 2000 MCE design spectra are also shown for each site.

Conclusions

The results and discussion in previous chapters indicate that application of IBC 2000 code procedures can be ambiguous, for place like Columbia, SC and can lead to under estimation of site response in some cases.

The basic reasons for this short-coming involve the generic non-hard-rock site conditions assumed for the USGS National Seismic Hazard Maps (Frankel et al., 2002), and the use of V_s, average shear wave velocity in the upper 30 m, as the basis for construction of response spectra as prescribed in IBC (2000).

The USGS National Seismic Hazard Maps assume a generic soil site response condition instead of a hard-rock condition. For site specific dynamic analysis, this assumed site response should be corrected for or removed altogether at sites similar to those studied here, where hard rock conditions exist in the shallow subsurface. Compounding the difficulty of rational application of the IBC 2000 code procedure is the fact that the average shear wave velocity in the upper 30 meters is used to scale the response spectrum. The procedure does not, in any way, account for the common situation wherein a transition for soil to hard-rock occurs within the 30 depth range. Thus, the profound amplification effects of a strong soil-rock impedance contrast in the shallow subsurface is not taken into consideration, leading to the potential for unconservative design at sites similar to those studied here.

As demonstrated in this study, site response analysis, following code procedures and parallel analysis using a geologically realistic model of the subsurface, can lead to very different results. The presence of a geologically realistic velocity gradient makes a significant impact on the calculated surface motions. The shear wave velocity in the transition zone from soil to rock is difficult to determine and may require using several geophysical and geotechnical methods, seismic reflection, seismic refraction, seismic crosshole, etc., in conjunction with CPT, to better resolve material properties.

The site classification, based on V_s (average soil shear wave velocity in the upper 30 meters), may not be a good indicator of site response. The four sites in Columbia, South Carolina are not an atypical situation, and are common throughout the central and eastern United States, where shallow soil overlies crystalline bedrock or Paleozoic sedimentary rock. In such cases, the impedance ratio is very high. As shown in chapter 5, site 2, classified as a "safer" site according to V_s, had the highest spectral acceleration values of the four sites investigated.

The IBC (2000) code is a general building code and as such cannot be expected to handle all site-specific conditions that may be encountered. The sites studied here are special, in the sense that they represent a class of site wherein a soil to hard-rock transition exists within 30 m of the ground surface. The fact that the IBC (2000) procedure underestimates response for such sites does not negate the utility of the code: it simply points to an area in which the code procedure needs improvement.

It is recommend that other site specific parameters, e.g. impedance ratio, depth to bedrock, should be incorporated into the site classification and design procedures. For example, Rodriguez-Marek et al. (2001) suggest an alternate site classification scheme that includes the depth to bedrock and a more diverse range of materials. Several major urban areas in the Eastern United States lie along the Fall Line (Raleigh, NC, Richmond, VA, Washington, DC, Baltimore, MD) and it is likely that there are many more sites, like site 2 in Columbia, South Carolina, that have great potential to amplify incoming seismic motion.

References:

Algermissen, S.T. and D. M. Perkins, (1976). "A Probabilistic Estimate of Maximum Acceleration in Rock in the Contiguous United States", U.S. Geological Survey, Open File Report 76-416

Ang, A. H. and Tang, W. H., (1975). Probability Concepts in Engineering Planning and Design: Volume 1 – Basic Principles; John Wiley & Sons, Inc., New York, pp. 114

Assimaki, D., Kausel, E., Whittle, A., (2000). "Model for dynamic shear modulus and damping for granular soils", *Journal of Geotechnical and Geoenvironmental Engineering, ASCE*, **126,** 859-869

Atkinson, G.M. and D.M. Boore, (1995). "Ground motion relations for Eastern North America", *Bulletin of Seismological Society of America*, 85, 17-30

Bakun, W.H. and M.G. Hopper (2004). "Magnitudes and Locations of the 1811-1812 New Madrid, Missouri, and the 1886 Charleston, South Carolina, Earthquakes", *Bulletin of the Seismological Society of America*, 94, pp. 64-75

Behrendt, J.C., R.M. Hamilton, H.D. Ackerman, V.J. Henry and K.C. Bayer, (1983). "Marine multichannel seismic-reflection evidence for Cenozoic faulting and deep crustal structure near Charleston, South Carolina" in Studies Related to the Charleston, South Carolina, Earthquake of 1886 – Tectonic and Seismicity, G. Gohn, editor, U.S. Geological Survey Professional Paper 1313, p. J1-J29

Beresnev, I.A., A.M., Nightengale and W.J. Silva, (2002). "Properties of Vertical Ground Motions", *Bulletin of the Seismological Society of America*, 92, 3152-3164

Bollinger, G.A., (1977). "Reinterpretation of the intensity data for the 1886 Charleston, South Carolina, earthquake" in Studies Related to the Charleston, South Carolina, Earthquake of 1886—A Preliminary Report, D. Rankin, editor, U.S.Geological Survey Professional Paper 1028, B17-B32

Boore, D.M. and G.M. Atkinson, (1987). "Stochastic Prediction of Ground Motion and Spectral Response Parameters at Hard-Rock Sites in Eastern North America", *Bulletin of Seismological Society of America*, 77, 440-467

Boore, D.M., (1983). "Stochastic Simulation of High-frequency Ground Motions Based on Seismological Models of the Radiated Spectra", *Bulletin of Seismological Society of America*, 73, 1865-1894

Boore, D.M., (1996). "SMSIM – Fortran programs for simulating ground motions from earthquakes: version 1", U.S. Geological Survey, Open File Report 96-80-A

Brune, J.N., (1970). "Tectonic Stress and the Spectra of Seismic Shear Waves from Earthquakes", *Journal of Geophysical Research*, 75, 4997-5010

Brune, J.N., (1971). "Correction", Journal of Geophyscial Research, 76, 5002

Campbell, K. W. (2003). "Prediction of Strong Ground Motion Using the Hybrid Empirical Method and Its Use in the Development of Ground-Motion (Attenuation) Relations in Eastern North America", *Bulletin of Seismological Society of America,* 93, 1012-1033

Chapman, M.C., G.A. Bollinger, M.S. Sibol, and D.E. Stephenson (1990). "The influence of the Coastal Plain Sedimentary Wedge on Strong Ground Motions from the 1886 Charleston, South Carolina, Earthquake", *Earthquake Spectra*, 6, No. 4, 617-640

Chapman, M.C., (1995). "A Probabilistic Approach to Ground-Motion Selection for Engineering Design", *Bulletin of Seismological Society of America,* 85, 937-942

Chapman, M.C. (2004). Revision of SHAKE91 Program.

Cook, F. A., Albaugh, D. S., Brown, L. D., Kaufman, S., Oliver, J. E. and Hatcher R. D., (1979). "Thin-skinned tectonics in the crystalline southern Appalachains, COCORP seismic reflection profiling of the Blue Ridge and Piedmont", *Geology*, v. 7, p. 563-567.

Cornell, C. A., (1968)."Engineering Seismic Risk Analysis", *Bulletin of Seismological Society of America*, 58, 1583-1606

Coruh, C., J.K. Costain, R. T. Williams, R. A. Phinney, R.D. Hatcher, Jr., and T.L. Pratt, (1987). "Results from regional vibroseis profiling: Appalachain ultra-deep corehole site study" (ADCOH), *Geophysical Journal of the Royal Astronomical Society*, 89, 147-156

Dobry, R. and M. Vucetic, (1987). "State of the art report: Dynamics properties and response of the soft clay deposits", from Proceedings of the International Symposium on Geotechnical Engineering Soft Soils, 2, 51-87

Dutton, C.E. (1889). The Charleston earthquake of August 31, 1886. U.S. Geological Survey, Ninth Annual Report, 1887-1888, 203-528

Frankel, A., (1995). "Mapping Seismic Hazard in the Central and Eastern United States", *Seismological Research Letters*, 66, 8-21

Frankel, A., C. Mueller, T. Barnhard, D. Perkins, E.V. Leyendecker, N. Dickman, S. Hanson and M. Hopper, (1996). "National Seismic-Hazard Maps: Documentation June 1996", U.S. Geological Survey Open-File Report 96-532

Frankel, A., M.D. Petersen, C.S. Mueller, K.M. Haller, R.L. Wheeler, E.V. Leyendecker, R.L. Wesson, S.C. Harmsen, C.H. Cramer, D.M. Perkins and K.S. Rukstales, (2002).

"Documentation of the 2002 Update of the National Seismic Hazard Maps", U.S. Geological Survey Open-File Report 02-420

Federal Emergency Management Agency, (1997). NEHRP Recommended Programs for Seismic Regulations for New Buildings and other Structures, Part 1: Provisions, FEMA 302, prepared by Building Seismic Safety Council, Washington, DC, 337 p.

Federal Emergency Management Agency. (2004). website: http://www.fema.gov/hazards/earthquakes/nehrp/index

Gutenberg, B. and C. F. Richter, (1954). Seismicity of the Earth, Princeton University Press, Second Edition, pp. 16-25

Hamburger, R.O. and C.A. Kircher, (2000). "Recent Developments in Seismic Design Methodologies and Codes", Earthquake Spectra, 16, vii-xiii

Hamilton, R. M., J.C. Behrendt and H.D. Ackermann, (1983). "Land multichannel seismic-reflection evidence for the tectonic features near Charleston, South Carolina", in Studies Related to the Charleston, South Carolina, Earthquake of 1886 – Tectonic and Seismicity, G. Gohn, editor, U.S. Geological Survey Professional Paper 1313, p. I1-I18

Hanks, T. C. and R. K. McGuire, (1981)."The Character of High-Frequency Strong Ground Motion", *Bulletin of Seismological Society of America*, 71, 2071-2095

Hartzell, S., L.F. Bonilla and R. A. Williams, (2004). "Prediction of Nonlinear Soil Effects", *Bulletin of Seismological Society of America*, 94, 1609-1629

Hatcher, R. D. Jr., (1987). "Tectonics of the southern and central Appalachian internides", *Annual review of earth and planetary sciences*, 15, 337-362

Hatcher, R.D. Jr. and S.A. Goldberg (1991). "The Blue Ridge Geologic Province", The Geology of the Carolinas, edited by J.W. Horton, Jr. and V.A. Zullo, The University of Tennessee Press: Knoxville, TN, p. 11-37

Hazel, J.E., L.M. Bybell, R. A. Christopher, N. O. Frederiksen, F. E. May, D. M. McLean, R. Z. Poore, C. C. Smith, N. F. Sohl, P. C. Valentine, and R. J. Witmer, (1977). "Biostratigraphy of the Deep Corehole (Clubhouse Crossroads Corehole 1) Near Charleston, South Carolina" in Studies Related to the Charleston, South Carolina, Earthquake of 1886—A Preliminary Report, D. Rankin, editor, U.S.Geological Survey Professional Paper 1028, F71-F89

Horton, J.W., Jr. and K.I. McConnell, (1991). "The Western Piedmont" in The Geology of the Carolinas, edited by J.W. Horton, Jr. and V.A. Zullo, The University of Tennessee Press: Knoxville, TN, 36-58

International Code Council. (2004) website: http://www.iccsafe.org/news/about/

International Building Code (2000). Section 1615, pp. 331-354

Ishibashi, I. and X. Zhang, (1993). "Unified Dynamic Shear Moduli and Damping Ratios of Sand and Clay", *Soils and Foundations*, 33, 182-191

Johnston, A.C. (1996). "Seismic moment assessment of earthquakes in stable continental regions, III: New Madrid 1811-1812, Charleston 1886, and Lisbon 1755", *Geophysical Journal International,* 126, 314-344

Knopoff, L., "A Matrix Method for Elastic Wave Problems", *Bulletin of Seismological Society of America*, 54, 431-438

Kramer, S. L., Geotechnical Earthquake Engineering, New Jersey: Prentice-Hall, 1996, p.175-178, 345

Lennon, G., (1986). "Identification of a northwest trending seismogenic graben near Charleston, South Carolina", U.S. Nuclear Regulatory Comission Report NUR-EG/CR-4705, 1-43

Marple, R.T. and P. Talwani, (2000). "Evidence for a buried fault system in the Coastal Plain of the Carolinas and Virginia—Implications for neotectonics in the southeastern United States", *Geological Society of America Bulletin*, 112, 200-220

Martin, G.R. and R. Dobry, (1994). "Earthquake site response and seismic code provisions, *NCEER Bulletin*, 8, 1-6

Maybin, A.H. and P.G. Nystrom, Geologic and Resource Map of South Carolina, 1997, SC Geological Survey and SC MAPS Education Program

Morrison, Phil, (2004). Personal Communication.

Munsey, J.W., (2004). "Seismic Hazard Assessment for the Tennessee Valley", Seismological Society of America Eastern Section Meeting 2004, Program with Abstracts

McGuire, R.K., (1995). "Probabilistic Seismic Hazard Analysis and Design Earthquakes: Closing the Loop", *Bulletin of Seismological Society of America*, 85, 1275-1284

Odum, J.K, R. A. Williams, W. J. Stephenson and D. M. Worley, (2003). "Near-Surface S-wave and P-wave Seismic Velocities of Primary Geological Formations on the Piedmont and Atlantic Coastal Plain of South Carolina, USA", U. S. Geological Survey Open File Report, OFR 03-043, 13 p.

Olgun, G., (2004). Personal Communication.

Olsen, K.B., (2000). "Site Amplification in the Los Angeles Basin from Three-Dimensional Modeling of Ground Motion", *Bulletin of Seismological Society of America*, 90, 77-94

Olsen, P.E., A.J. Froelich, D.L. Daniels, J.P. Smoot and P.J.W. Gore (1991). "Rift Basins of Early Mesozoic Age", The Geology of the Carolinas. The University of Tennessee Press: Knoxville, TN, pp. 142-170

Overstreet, W. C. (1970). "The Piedmont in South Carolina", Studies of Appalachain Geology. John Wiley & Sons: New York, NY. pp. 369-382

Rankin, D.W. (1977). "Studies Related to the Charleston, South Carolina, Earthquake of 1886—Introduction and Discussion" in Studies Related to the Charleston, South Carolina, Earthquake of 1886—A Preliminary Report, D. Rankin, editor, U.S.Geological Survey Professional Paper 1028, A1-A15

Reed, J.C., Jr., B. Bryant, and W.B. Myers, (1970). "The Brevard Zone: A Reinterpretation" in Studies of Appalachian Geology, John Wiley & Sons: New York, 261-269

Reid, H.F., (1910). The California Earthquake of April 18, 1906, Report of the state earthquake investigation commission, Vol II, The Mechanics of the earthquake, Carnegie Institution of Washington, Publication No. 87, Vol. II, 192 p.

Rodriguez-Marek, A., J.D. Bray, N.A. Abrahamson, (2001). "An Empirical Geotechnical Seismic Site Response Procedure", *Earthquake Spectra*, 17, 65-87

Schilt, F. S., L.D. Brown, J.E. Oliver and S. Kaufman, (1983). "Subsurface Structure Near Charleston, South Carolina – Results of the COCORP Reflection Profiling in the Atlantic Coastal Plain" in Studies Related to the Charleston, South Carolina, Earthquake of 1886 – Tectonic and Seismicity, G. Gohn, editor, U.S. Geological Survey Professional Paper 1313, p. H1-H19

Schnabel, P., Seed, H. Bolton, and Lysmer, 1972, "Modification of Seismograph Records for Effects of Local Soil Conditions", *Bulletin of Seismological Society of America,* 62, 1649-1664

Schnabel, P., Seed, H. Bolton, and Lysmer, 1973, Erratum, *Bulletin of Seismological Society of America,* 63, 750

Schnabel, P. B., Lysmer, J. and Seed, H.B., 1972. SHAKE: A Computer Program for Earthquake Response Analysis of Horizontally Layered Sites. Report No. EERC 72-12, College of Engineering, University of California, Berkeley, California, 88 p.

Schwartz, D. P and K.J. Coppersmith, (1984). "Fault behavior and characteristic earthquakes: examples from the Wasatch and San Andreas faults*", Journal of Geophysical Research*, 89, 5681-5698

Shearer, P.M. and J. A. Orcutt, (1987). "Surface and near-surface effects on seismic waves—theory and borehole seismometer results", *Bulletin of Seismological Society of America,* 77, 1168-1196

Singh, S. K., J. Lermo, T. Domingues, M. Ordaz, J.M. Espinosa, E. Mena and R. Quaas, (1988). "The Mexico Earthquake of September 19, 1985 – A Study of Amplification of Seismic Waves in the Valley of Mexico with Respect to a Hill Zone Site", *Earthquake Spectra*, Vol. 4, No. 4

Snipes, D.S.,W.C. Fallaw, Van Price Jr. and R.J. Cumbest, (1993). "The Pen Branch Fault: Documentation of Late Cretaceous-Tertiary Faulting in the Coastal Plain of South Carolina", *Southeastern Geology*, 33, No.4, 195-218

Somerville, P., N. Collins, N. Abrahamson, R. Graves, and C. Saikia, (2001), Ground motion attenuation relations for the central and eastern United States, final report to U.S. Geological Survey

Southeastern U.S. Seismic Network Operators, (2004). The Southeastern United States Seismicity Catalog, Virginia Tech Seismological Observatory, Blacksburg, Virginia

Talwani, P., (1982). "An internally consistent pattern of seismicity near Charleston, South Carolina", *Geology*, 10, 655-658

Talwani, P., (1999). "Fault geometry and earthquakes in continental interiors", *Tectonophyisics*, 305, 371-379

Talwani, P. and W.T. Schaffer, (2001). "Recurrence rates of large earthquakes in the South Carolina Coastal Plain based on paleoliquefaction data", *Journal of Geophysical Research*, 106, 6621-6642.

Toro, G., N. Abrahamson, and J. Schneider, (1997). Model of strong ground motions from earthquakes in the central and eastern North America: best estimates and uncertainties", *Seismological Research Letters*, 68, 41-57

Vucetic, M. and R. Dobry, (1991). "Effect of Soil Plasticity on Cyclic Response", *Journal of Geotechnical Engineering*, 11, 59-68

Weems, R. E., E.M. Lemon, Jr., and E.D. Cron, (1997). "Geology of the Pringletown, Ridgeville, Summerville, and Summerville Northwest 7.5-minute quadrangles, Berkeley, Charleston and Dorchester Counties, South Carolina: U.S. Geological Survey Miscellaneous Investigations Map 2502, scale 1:24000, text.

Weems, R. E. and Lewis, W.C. (2002). "Structural and tectonic setting of the Charleston, South Carolina, region: Evidence from the Tertiary stratigraphic record", *Geological Society of America Bulletin*, 114, 24-42

Wikipedia. (2004). Website: http://en.wikipedia.org/wiki/Building_code

Yantis, B. R., J.K. Costain and H.D. Ackermann, (1983). "A Reflection Seismic Study Near Charleston, South Carolina" in Studies Related to the Charleston, South Carolina, Earthquake of 1886—A Preliminary Report, G. Gohn, editor, U.S. Geological Survey Professional Paper 1313, p.G1-G20

Youngs, R. R. and K.J. Coppersmith, (1985). "Implications of Fault Slip Rates and Earthquake Recurrence Models to Probabilistic Seismic Hazard Estimates", *Bulletin of Seismological Society of America,* 75, 939-964